AMERICAN SOCIETY FOR MICROBIOLOGY | mBio®

RESEARCH ARTICLE

# Homeobox Transcription Factors Are Required for Fungal Development and the Suppression of Host Defense Mechanisms in the *Colletotrichum scovillei*-Pepper Pathosystem

**Teng Fu,[a] Joon-Hee Han,[b] Jong-Hwan Shin,[a] Hyeunjeong Song,[c] Jaeho Ko,[c] Yong-Hwan Lee,[c] Ki-Tae Kim,[d] Kyoung Su Kim[a]**

[a]Division of Bio-Resource Sciences, BioHerb Research Institute, and Interdisciplinary Program in Smart Agriculture, Kangwon National University, Chuncheon, South Korea

[b]Department of Research and Development, Chuncheon Bioindustry Foundation, Chuncheon, South Korea

[c]Department of Agricultural Biotechnology, Interdisciplinary Program in Agricultural Genomics, Center for Fungal Genetic Resources, Plant Immunity Research Center, and Research Institute of Agriculture and Life Sciences, Seoul National University, Seoul, South Korea

[d]Department of Agricultural Life Science, Sunchon National University, Suncheon, South Korea

**ABSTRACT** *Colletotrichum scovillei*, an ascomycete phytopathogenic fungus, is the main causal agent of serious yield losses of economic crops worldwide. The fungus causes anthracnose disease on several fruits, including peppers. However, little is known regarding the underlying molecular mechanisms involved in the development of anthracnose caused by this fungus. In an initial step toward understanding the development of anthracnose on pepper fruits, we retrieved 624 transcription factors (TFs) from the whole genome of *C. scovillei* and comparatively analyzed the entire repertoire of TFs among phytopathogenic fungi. Evolution and proliferation of members of the homeobox-like superfamily, including homeobox (HOX) TFs that regulate the development of eukaryotic organisms, were demonstrated in the genus *Colletotrichum*. *C. scovillei* was found to contain 10 HOX TF genes (*CsHOX1* to *CsHOX10*), which were functionally characterized using deletion mutants of each *CsHOX* gene. Notably, *CsHOX1* was identified as a pathogenicity factor required for the suppression of host defense mechanisms, which represents a new role for HOX TFs in pathogenic fungi. *CsHOX2* and *CsHOX7* were found to play essential roles in conidiation and appressorium development, respectively, in a stage-specific manner in *C. scovillei*. Our study provides a molecular basis for understanding the mechanisms associated with the development of anthracnose on fruits caused by *C. scovillei*, which will aid in the development of novel approaches for disease management.

**IMPORTANCE** The ascomycete phytopathogenic fungus, *Colletotrichum scovillei*, causes serious yield loss on peppers. However, little is known about molecular mechanisms involved in the development of anthracnose caused by this fungus. We analyzed whole-genome sequences of *C. scovillei* and isolated 624 putative TFs, revealing the existence of 10 homeobox (HOX) transcription factor (TF) genes. We found that *CsHOX1* is a pathogenicity factor required for the suppression of host defense mechanism, which represents a new role for HOX TFs in pathogenic fungi. We also found that *CsHOX2* and *CsHOX7* play essential roles in conidiation and appressorium development, respectively, in a stage-specific manner in *C. scovillei*. Our study contributes to understanding the mechanisms associated with the development of anthracnose on fruits caused by *C. scovillei*, which will aid for initiating novel approaches for disease management.

**KEYWORDS** anthracnose, appressorium development, *Colletotrichum scovillei*, conidiation, host defense, pathogenicity factor

**Citation** Fu T, Han J-H, Shin J-H, Song H, Ko J, Lee Y-H, Kim K-T, Kim KS. 2021. Homeobox transcription factors are required for fungal development and the suppression of host defense mechanisms in the *Colletotrichum scovillei*-pepper pathosystem. mBio 12:e01620-21. https://doi.org/10.1128/mBio.01620-21.

**Editor** B. Gillian Turgeon, Cornell University



Address correspondence to Ki-Tae Kim, kitaekim@scnu.ac.kr, or Kyoung Su Kim, kims@kangwon.ac.kr.

**Received** 1 June 2021
**Accepted** 20 July 2021
**Published** 24 August 2021

Pepper (*Capsicum annuum* L.) is an important vegetable crop cultivated in nearly all countries worldwide (1). The yearly worldwide pepper production has been estimated at approximately 36.8 million tons (2). Peppers have been widely used as a food flavoring agent and as medicine for thousands of years. Peppers are good sources of vitamins and minerals; they contain multiple chemical constituents with pharmaceutical properties (1). A major hindrance in pepper production is anthracnose disease caused by *Colletotrichum* species, which are ascomycete fungal pathogens. Anthracnose refers to diseases with the typical symptoms of sunken spots or lesions on infected plant tissues (3, 4). The disease causes substantial economic losses by reducing the productivity and quality of fruits in affected plants (5). Several species in the genus *Colletotrichum* are known to cause anthracnose in pepper plants (6–8). Among them, *C. scovillei*, which belongs to the *Colletotrichum acutatum* species complex, is considered a dominant pathogen responsible for serious pepper yield losses in countries in tropical and temperate zones, including Brazil, China, Indonesia, Japan, South Korea, Malaysia, and Thailand (9–15). *C. scovillei* has also been reported to attack other economically important crops, such as mango and banana (16, 17). Although most anthracnose disease on fruits can cause considerable losses in yield and quality, the molecular mechanism underlying the development of fruit anthracnose has not yet been elucidated, whereas many foliar diseases in a wide range of plants caused by diverse fungal pathogens have been extensively studied at the molecular level (18–24). Therefore, we have initiated a molecular pathosystem study of *C. scovillei* and pepper fruits to better understand anthracnose disease in fruit.

*C. scovillei* produces a large number of conidia that serve as a major inoculum. During the disease cycle, conidia adhere to the surfaces of pepper fruits upon hydration; they then produce germ tubes (7, 25). Appressorium, a specialized infection structure, is differentiated at the tip of the germ tube following the recognition of chemical and physical host signals (26). Considering that *C. scovillei* infects only the fruit, the signals for appressorium development on fruit are different from the signals for appressorium development on other tissues of host plants. Similar to several *Colletotrichum* species, *C. scovillei* is a hemibiotroph, which exhibits an early biotrophic phase and a late necrotrophic phase during host-pathogen interactions (6, 26–28). At an early stage of appressorium-mediated penetration of *C. scovillei*, a unique feature known as a dendroid structure develops in the cuticle layer of pepper fruit; this does not occur in foliar infections involving other *Colletotrichum* pathogens (4, 29, 30). After colonization of host epidermal cells, the fungus develops the typical sunken anthracnose lesion with mucilaginous acervuli containing a large amount of pinkish conidia, which is important for further infection. Polycyclic infection of the fungus contributes to substantial disease during the growing season, thereby causing serious economic losses. Based on the socioeconomic impact and difficulty involved in disease management of fruit anthracnose in a wide range of crops, we previously elucidate the whole genome of *C. scovillei* to better understand the molecular mechanisms involved in fruit anthracnose, which have been relatively uncharacterized at the molecular level (8, 31, 32).

Eukaryotic organisms, including fungi, have evolved adaptive genetic responses to a variety of stimuli (33, 34). Transcription factor (TF)-mediated regulation of gene expression plays an important role in controlling crucial aspects of organism survival and development. Gene expression is elaborately orchestrated in a coordinated system of transcription-mediated signaling, in which TFs bind specific sequence elements to initiate or block transcription (35–37). Various TF families are defined by unique DNA-binding motifs (38–40). Although the DNA-binding motifs of TF families are highly conserved across taxa, the members of a particular TF family often have different roles in an organism because of evolutionary divergence (41–43). The availability of genome sequence data has resulted in the identification of a large number of TFs through cross-species comparison, thus enabling TF family-based characterization in functional genomics (44). The homeobox TF family is a prominent TF family associated with fungal development and pathogenicity. Members of this family contain a conserved

60-amino-acid DNA-binding motif known as the homeodomain (45, 46). Since the functional discovery of the homeobox TF family in *Drosophila melanogaster*, which is expressed in an organ-specific manner during development (47, 48), important roles of homeobox TF orthologs have been established in several fungi (33, 49–52). For example, the rice blast fungal pathogen *Magnaporthe oryzae* contains seven homeobox TFs, among which *MoHOX2* and *MoHOX7* have been identified as stage-specific key regulators of conidiation and appressorium development, respectively (33, 53). Functional roles of homeobox TFs in infection-related development have been demonstrated in *Colletotrichum orbiculare*, a cucumber anthracnose pathogen, which is evolutionarily very distant from *C. scovillei* (54, 55). Unlike *MoHOX7*, the homolog *CoHox3* was associated with maturation of appressoria in *C. orbiculare*. *CoHOX1* was found to be required for pathogenic development, whereas its homolog *MoHOX5* was dispensable for pathogenicity. These results reflect the functional divergence of homeobox TF family members, which further increases the genetic complexities of fungal pathogens with different lifestyles, in response to a wide variety of environmental signals. However, the HOX TF family in pepper fruit anthracnose *C. scovillei* has not yet been studied.

To systematically study the functions of *HOX* genes, we first analyzed whole-genome sequences of *C. scovillei* and isolated 624 putative TFs (based on InterPro annotation), which contain 48 distinct domains. Through detection of the homeobox domain (IPR001356), a total of 10 HOX TFs (CsHOX1 to CsHOX10) were then obtained from putative TFs in *C. scovillei*. These HOX TFs in the homeobox-like domain superfamily (IPR009057) were evolutionarily analyzed in the *Colletotrichum* genus and outgroup species to reveal their origins. To further study the functional roles of *CsHOX* genes in *C. scovillei*, we then generated deletion mutants for each *CsHOX* gene, based on homology-dependent gene replacement. Comparative functional analysis of deletion mutants demonstrated that *CsHOX* genes are associated with stage-specific regulations for disease dissemination and development in *C. scovillei*. Specifically, *CsHOX2*, *CsHOX7*, and *CsHOX1* were found to be essential for conidiation, appressorium formation, and suppression of the host defense mechanism for anthracnose development on pepper fruits in the *C. scovillei*-host pathosystem, respectively. Our findings provide a useful framework for understanding the development of anthracnose disease on fruits caused by *Colletotrichum* species.

## RESULTS

**Distribution of TF and homeobox-related proteins in fungal species including *Colletotrichum* spp.** Our phylogenomic species tree of *Colletotrichum* was consistent with previous phylogenetic trees (56, 57) (see Fig. S1A and Table S1A in the supplemental material). The *C. acutatum* species complex diverged from *Colletotrichum orchidophilum*, as previously reported (56). The total number of TFs in *Colletotrichum* species ranged from 337 in *Colletotrichum chlorophyti* to 624 in *C. scovillei* (see Fig. S1A and Table S1B and C). The average number of TFs in this genus was 437.0, which was higher than the average number of TFs in the sister taxon *Verticillium* (316.5) but considerably less than the average number of TFs in the distantly related taxon *Fusarium* (985.7). Among the TFs, the average number of genes encoding a protein with a homeobox-like domain was 46.3 in all selected species (see Table S1D). However, *C. scovillei* in the *Colletotrichum* genus and outgroup species, including *Fusarium verticillioides*, *Fusarium oxysporum*, and *Sclerotinia sclerotiorum*, had significantly higher numbers of genes than average at 206, 77, 73, and 126 genes, respectively. In contrast, the number of *HOX* genes in the *Colletotrichum* genus consistently ranged from 8 to 11, whereas the number in the outgroup species exhibited considerable variability, from 2 in *Saccharomyces pombe* to 27 in *F. verticillioides* (see Table S1E). These results indicated that plant pathogens possess more TFs and *HOX* genes than saprotrophs.

In total, 104 different types of structures were observed in proteins with homeobox-like domains in the selected fungal species (see Table S1F). Among them, 13 types were proteins with a homeobox domain, although only eight types were detected in *Colletotrichum* species (see Fig. S1B). Within *Colletotrichum* species, proteins that only

contained a homeobox domain were most frequently detected. The next most commonly detected HOX proteins had at least two or three $C_2H_2$-type zinc finger domains (IPR007087). A HOX protein with rhodanese-like domain (IPR036873) was present in all members of the *C. acutatum* species complex, but sparsely present in other *Colletotrichum* species. Some HOX proteins with $C_2H_2$-type zinc finger domains also had an HTH CenpB-type DNA-binding domain (IPR006600), and were also present in all *Colletotrichum* species, except *Colletotrichum tanaceti*. *C. orbiculare* contained one of these proteins, with an additional DUF3425 domain (IPR021833) at the C-terminal end. A HOX protein with three $C_2H_2$-type zinc finger domains, NAD(P)-binding domain (IPR036291), and 6-phosphogluconate dehydrogenase-like C-terminal domain (IPR008927) was only present in *Colletotrichum salicis*.

**Evolution and proliferation of the homeodomain superfamily and *HOX* genes in fungal species, including *Colletotrichum* spp.** Gain and loss analysis of genes encoding members of the homeodomain superfamily, including the *HOX* genes, showed that 35 ancestral genes existed in the last common ancestor of the *Colletotrichum* species complex (see Fig. S1C). The last common ancestor of the *C. acutatum* species complex had 37 genes, which remain in *Colletotrichum simmondsii*, *C. salicis*, and *C. orchidophilum*, while 1 and 2 genes were lost in *Colletotrichum nymphaeae* and *Colletotrichum fioriniae*, respectively. Overall, the phylogenetic tree of the homeodomain superfamily showed that the superfamily of the selected fungal species was divided into 17 clades (see Fig. S1D and Table S1G). The largest clade had 809 genes (clade 15), while the second-largest clade had 211 genes (clade 10); both contained proteins with homeobox domains. Clades 10 and 15 had 148 and 153 *HOX* genes, respectively, which formed a subclade within each clade (see Fig. S1D). The subclades of clades 10 and 15 were further divided into 14 and six families, respectively (see Fig. S1E and S1F). Each subclade contained five *HOX* genes of *C. scovillei*. Although subclade 15 only consisted of *HOX* genes, subclade 10 contained a highly diverged homeobox-like domain family (family 3). A pair of *HOX* genes from *Colletotrichum tofieldiae* (KZL74285.1) and *Colletotrichum incanum* (OHW97559.1) (family 2), and a pair of *HOX* genes from *Colletotrichum gloeosporioides* (EQB57487.1) and *Colletotrichum fructicola* (ELA29112.1) (family 10), each independently formed their own families (see Fig. S1E).

Another notable feature of the tree was that the genes encoding proteins with homeobox-like domains in *C. scovillei* and *S. sclerotiorum* were extensively proliferated in a subclade within clade 15 (see Fig. S1D). This proliferation of genes appeared to be primarily caused by the DNA transposon TcMar-Fot1 in both fungi (see Fig. S2A). Without these duplicated genes, *C. scovillei* only contained 36 homeodomain superfamily genes, similar to its sister species *C. nymphaeae* (see Fig. S1C). Unlike *HOX* genes and the homeodomain superfamily sparsely scattered in the genome of *C. scovillei*, these genes were located in clusters throughout the genome (see Fig. S2B). This phenomenon may be driven by the activity of a DNA transposon.

As representatives of nuclear localization of HOX TFs in *C. scovillei*, we confirmed nuclear localization of CsHOX2 and CsHOX7 using transformants expressing the fusion proteins CsHOX2:sGFP and CsHOX7:sGFP, respectively, during fungal development (see Fig. S2C and S2D). HOX proteins of *C. scovillei* have been compared to known HOX proteins of *M. oryzae* and *S. cerevisiae* (33, 58). While *S. cerevisiae* has nine HOX protein-encoding genes, *M. oryzae* has seven; *C. scovillei* has three genes, in addition to the seven present in *M. oryzae* (see Fig. S2A). All HOX proteins in *C. scovillei* were found to be orthologous to those in *M. oryzae*, with the exceptions of CsHOX3, CsHOX8, CsHOX9, and CsHOX10. The homeobox domain in CsHOX8 with two $C_2H_2$ zinc finger domains and an HTH CenpB-type DNA-binding domain and CsHOX9 without any other domains were found to be paralogous to each other (see Fig. S2A). Only two *C. scovillei* proteins, CsHOX6 and CsHOX7, were found to be orthologous to the *HOX* genes in *S. cerevisiae* and *M. oryzae*.

**Generation of *CsHOX*-deletion mutants in *C. scovillei*.** To investigate the functional roles of *CsHOX* genes during fungal developments and infection of *C. scovillei*, we generated deletion mutants (Δ*Cshox1* to Δ*Cshox10*) for each *CsHOX* gene via

**TABLE 1** Phenotypic characterization of *CsHOX* gene deletion mutants in *C. scovillei*[a]

| Strain | Growth (mm)[b] | | Conidiation ($10^4$/ml)[c] | Conidial size ($\mu$m)[d] | | Conidial germination (%)[e] | Appressorium formation (%)[f] |
|---|---|---|---|---|---|---|---|
| | CMA | MMA | | Length | Width | | |
| Wild-type | 49.3 ± 0.3$^{A}$ | 44.3 ± 0.5$^{ABC}$ | 155.0 ± 9.1$^{A}$ | 10.9 ± 1.3$^{D}$ | 3.7 ± 0.5$^{B}$ | 97.5 ± 1.3$^{A}$ | 90.0 ± 3.2$^{A}$ |
| Δ*Cshox1* | 31.8 ± 0.5$^{E}$ | 24.5 ± 0.9$^{H}$ | 158.8 ± 12.9$^{A}$ | 19.9 ± 2.4$^{A}$ | 3.4 ± 0.3$^{C}$ | 81.0 ± 4.4$^{D}$ | 31.0 ± 6.7$^{B}$ |
| *Cshox1c* | 48.5 ± 0.6$^{A}$ | 44.0 ± 0.8$^{ABC}$ | 148.5 ± 9.8$^{A}$ | 10.6 ± 1.1$^{D}$ | 3.8 ± 0.5$^{B}$ | 97 ± 1.8$^{AB}$ | 90.5 ± 4.5$^{A}$ |
| Δ*Cshox2* | 42.3 ± 0.5$^{D}$ | 32.8 ± 0.9$^{G}$ | 0$^{D}$ | ND | ND | ND | ND |
| *Cshox2c* | 49.0 ± 0.8$^{A}$ | 44.3 ± 1.3$^{ABC}$ | 150.8 ± 6.4$^{A}$ | 11.0 ± 1.2$^{D}$ | 3.6 ± 0.3$^{B}$ | 94.8 ± 2.2$^{ABC}$ | 89.8 ± 5.1$^{A}$ |
| Δ*Cshox3* | 48.3 ± 0.3$^{A}$ | 44.0 ± 0.8$^{ABC}$ | 87.5 ± 6.5$^{C}$ | 15.1 ± 2.3$^{B}$ | 4.2 ± 0.3$^{A}$ | 92.0 ± 3.2$^{BC}$ | 88.8 ± 3.9$^{A}$ |
| *Cshox3c* | 48.8 ± 0.9$^{A}$ | 43.8 ± 0.5$^{ABCD}$ | 153.0 ± 13.5$^{A}$ | 10.9 ± 1.1$^{D}$ | 3.7 ± 0.4$^{B}$ | 96.8 ± 1.7$^{AB}$ | 89.3 ± 5.5$^{A}$ |
| Δ*Cshox4* | 44.5 ± 0.6$^{C}$ | 38.0 ± 0.8$^{F}$ | 150.5 ± 8.8$^{A}$ | 14.2 ± 1.2$^{C}$ | 4.4 ± 0.4$^{A}$ | 92.8 ± 2.2$^{ABC}$ | 89.5 ± 4.4$^{A}$ |
| *Cshox4c* | 48.8 ± 0.9$^{A}$ | 44.8 ± 0.5$^{AB}$ | 157.5 ± 13.0$^{A}$ | 11.0 ± 1.6$^{D}$ | 3.9 ± 0.4$^{B}$ | 95.8 ± 2.1$^{ABC}$ | 89.0 ± 4.0$^{A}$ |
| Δ*Cshox5* | 48.5 ± 0.6$^{A}$ | 41.5 ± 0.6$^{E}$ | 151.3 ± 7.0$^{A}$ | 15.7 ± 1.0$^{B}$ | 4.4 ± 0.3$^{A}$ | 90.5 ± 2.6$^{C}$ | 89.0 ± 5.0$^{A}$ |
| *Cshox5c* | 48.5 ± 0.6$^{A}$ | 44.5 ± 0.6$^{ABC}$ | 146.8 ± 4.7$^{A}$ | 10.9 ± 1.1$^{D}$ | 3.6 ± 0.4$^{B}$ | 95.3 ± 2.2$^{ABC}$ | 88.8 ± 5.9$^{A}$ |
| Δ*Cshox6* | 47.3 ± 0.5$^{B}$ | 43.3 ± 0.5 $^{CD}$ | 123.0 ± 6.3$^{B}$ | 10.6 ± 1.2$^{D}$ | 3.7 ± 0.4$^{B}$ | 95.5 ± 3.4$^{ABC}$ | 89.0 ± 5.4$^{A}$ |
| *Cshox6c* | 48.8 ± 0.9$^{A}$ | 44.3 ± 0.5$^{ABC}$ | 148.5 ± 6.0$^{A}$ | 10.9 ± 1.4$^{D}$ | 3.7 ± 0.4$^{B}$ | 94.8 ± 2.5$^{ABC}$ | 90.0 ± 5.4$^{A}$ |
| Δ*Cshox7* | 48.5 ± 0.6$^{A}$ | 42.5 ± 0.6$^{DE}$ | 156.8 ± 15.9$^{A}$ | 10.8 ± 1.3$^{D}$ | 3.8 ± 0.3$^{B}$ | 95.0 ± 2.2$^{ABC}$ | 0$^{C}$ |
| *Cshox7c* | 48.8 ± 0.7$^{A}$ | 43.8 ± 0.9$^{ABCD}$ | 150.0 ± 4.4$^{A}$ | 10.9 ± 1.6$^{D}$ | 3.8 ± 0.4$^{B}$ | 94.5 ± 3.4$^{ABC}$ | 89.3 ± 5.1$^{A}$ |
| Δ*Cshox8* | 48.0 ± 0.8$^{AB}$ | 42.3 ± 1.3$^{BCD}$ | 158.1 ± 9.8$^{A}$ | 11.0 ± 1.3$^{D}$ | 3.8 ± 0.3$^{B}$ | 95.8 ± 2.2$^{ABC}$ | 85.3 ± 4.3$^{AD}$ |
| *Cshox8c* | 48.8 ± 0.9$^{A}$ | 44.3 ± 0.9$^{ABC}$ | 154.3 ± 19.6$^{A}$ | 11.0 ± 1.2$^{D}$ | 3.6 ± 0.4$^{B}$ | 95.5 ± 2.1$^{ABC}$ | 90.3 ± 3.5$^{A}$ |
| Δ*Cshox9* | 48.0 ± 0.8$^{AB}$ | 43.3 ± 0.5 $^{CD}$ | 150.0 ± 7.7$^{A}$ | 11.0 ± 1.4$^{D}$ | 3.8 ± 0.3$^{B}$ | 95.3 ± 2.5$^{ABC}$ | 86.0 ± 3.7$^{AD}$ |
| *Cshox9c* | 48.8 ± 0.8$^{AB}$ | 45.0 ± 1.4$^{A}$ | 155.5 ± 14.8$^{A}$ | 11.0 ± 1.4$^{D}$ | 3.7 ± 0.4$^{B}$ | 94.5 ± 2.4$^{ABC}$ | 88.8 ± 6.2$^{A}$ |
| Δ*Cshox10* | 48.8 ± 0.9$^{A}$ | 43.8 ± 0.9$^{ABCD}$ | 141.8 ± 12.6$^{A}$ | 10.8 ± 1.3$^{D}$ | 3.7 ± 0.3$^{B}$ | 95.0 ± 2.2$^{ABC}$ | 89.8 ± 4.6$^{A}$ |
| *Cshox10c* | 49.0 ± 0.8$^{A}$ | 43.8 ± 0.9$^{ABCD}$ | 148.8 ± 9.4$^{A}$ | 11.1 ± 1.3$^{D}$ | 3.7 ± 0.3$^{B}$ | 94.5 ± 2.9$^{ABC}$ | 89.8 ± 5.0$^{A}$ |

[a]Data are presented as means ± the standard deviations of three independent experiments, with three replicates per experiment. Significant differences were estimated using Duncan's test ($P < 0.05$). The same superscript capital letters in a column indicate no significant difference. ND, not determined.
[b]Mycelial growth was measured at 6 days postinoculation on CMA and MMA.
[c]Conidiation was evaluated by counting the number of conidia collected with 5 ml of distilled water from 6-day-old V8 agar medium.
[d]Conidial size was determined by measuring the lengths and widths of at least 100 conidia.
[e]Percentage of conidial germination was measured at 12 h postinoculation on a hydrophobic surface using conidia from 6-day-old oatmeal agar. In each replicate, at least 100 conidia were measured.
[f]The percentage of appressorium formation was measured at 16 h postinoculation on a hydrophobic surface using conidia from 6-day-old oatmeal agar. In each replicate, at least 100 conidia were measured.

homology-dependent targeted gene replacement. The deletion mutants were confirmed by Southern blotting and RT-PCR (see Fig. S3). Compared to the wild-type strain of *C. scovillei*, the deletion mutants displayed altered phenotypes during fungal developments and pathogenicity (Table 1; see also Fig. S4A to D). Briefly, the Δ*Cshox2*, Δ*Cshox3*, and Δ*Cshox6* strains were reduced in conidiation; the Δ*Cshox1*, Δ*Cshox3*, Δ*Cshox4*, and Δ*Cshox5* strains produced abnormally morphological conidia; the Δ*Cshox1* and Δ*Cshox7* strains were impaired in appressorium formation in response to hydrophobic surface; the Δ*Cshox1*, Δ*Cshox7*, Δ*Cshox8*, and Δ*Cshox9* strains were defective in pathogenicity; the Δ*Cshox2* strain caused normal anthracnose disease through appressorium-like structures developed from tips of mycelia. Moreover, the wild-type strain was not found to produce conidiomata, whereas the Δ*Cshox1*, Δ*Cshox3*, Δ*Cshox5*, and Δ*Cshox6* formed conidiomata on artificial medium (see Fig. S4B).

***CsHOX* genes are important for conidium production.** Anthracnose disease of pepper by *C. scovillei* is quickly spread via conidia in favorable environmental conditions. Therefore, we evaluated the conidiation of *CsHOX* gene deletion mutants. Quantitative analysis of conidia showed that Δ*Cshox3* and Δ*Cshox6* were significantly defective in conidiation, compared to the wild-type and complemented strains (Table 1). Notably, Δ*Cshox2* was completely defective in conidiation, indicating that *CsHOX2* is essential for conidiation in *C. scovillei*. Microscopic investigation revealed that no conidia were observed in Δ*Cshox2* with prolonged incubation, while the wild-type and *Cshox2c* strains developed dense conidiophores bearing conidia in 5 h (Fig. 1A). To further determine whether *CsHOX2* is involved in conidiophore formation, lactophenol aniline blue was applied to distinguish conidiophores from aerial hyphae. Microscopic examination indicated that wild-type, Δ*Cshox2*, and *Cshox2c* strains developed conidiophores (Fig. 1B). Taken together, these results indicated that *CsHOX2* is a specific regulator of conidium

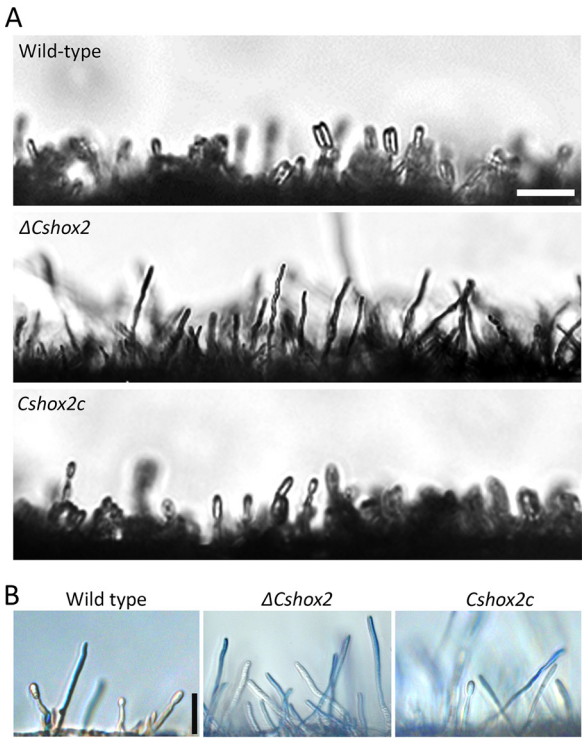


**FIG 1** *CsHOX2* is essential for conidium production. (A) Production of conidia from conidiophores under inductive conditions. Photographs were taken after incubation of 3-day-old mycelial agar plugs in a humid box with light for 5 h. Scale bar, 25 $\mu$m. (B) Conidiophore development under inductive conditions. Aerial hyphae (blue) were stained by lactophenol aniline blue; conidiophores were not stained. Scale bar, 25 $\mu$m.

production, and that *CsHOX3* and *CsHOX6* are quantitatively related to conidium production in *C. scovillei*.

***CsHOX* genes are related to the morphology and germination of conidium, and stress response.** Proper morphology and germination of conidium are prerequisites for efficient infection in conidium-mediated disease development. In terms of morphology, the Δ*Cshox1*, Δ*Cshox3*, Δ*Cshox4*, and Δ*Cshox5* mutants produced abnormal conidia, which were larger than the conidia of the wild-type and complemented strains (Fig. 2A and Table 1). This finding suggested that *CsHOX1*, *CsHOX3*, *CsHOX4*, and *CsHOX5* are important for conidial morphology. Conidial germination rates of the Δ*Cshox1*, Δ*Cshox3*, and Δ*Cshox5* strains were significantly reduced, indicating that *CsHOX1*, *CsHOX3*, and *CsHOX5* are involved both in conidial morphology and germination (Table 1). When fungicides (e.g., dimethomorph, oxolinic acid, carbendazim, and fludioxonil) were applied to conidial germination assays, conidial germination of the Δ*Cshox1* and Δ*Cshox4* strains was significantly reduced by stress with dimethomorph (1 or 0.1 ppm) and carbendazim (1 ppm), respectively, compared to the germination of the wild-type and corresponding complemented strains (see Fig. S5A). In addition, germ tubes and conidia of the Δ*Cshox1* strain displayed abnormal swelling following treatment with the chitin synthase inhibitor nikkomycin Z, compared to the wild-type and *Cshox1c* strains (see Fig. S5B). Moreover, we tested whether thermal stress affected the germination of conidia with abnormal morphology. The conidia of Δ*Cshox1*, Δ*Cshox3*, Δ*Cshox4*, and Δ*Cshox5* exhibited germination rates that were similar to the rate of the wild-type strain at 20°C, whereas the demonstrated significant inhibition of conidial germination at 32°C (Fig. 2B; see also Fig. S5C). Thus, we tested whether the conidial longevities of the Δ*Cshox1*, Δ*Cshox3*, Δ*Cshox4*, and Δ*Cshox5* strains were reduced by heat shock. Phloxine B was used to assess conidial survival. After incubation for 16 h, the ratios of conidial survival of Δ*Cshox1*, Δ*Cshox3*, Δ*Cshox4*, and Δ*Cshox5* strains were significantly reduced as the temperature increased from 25°C to

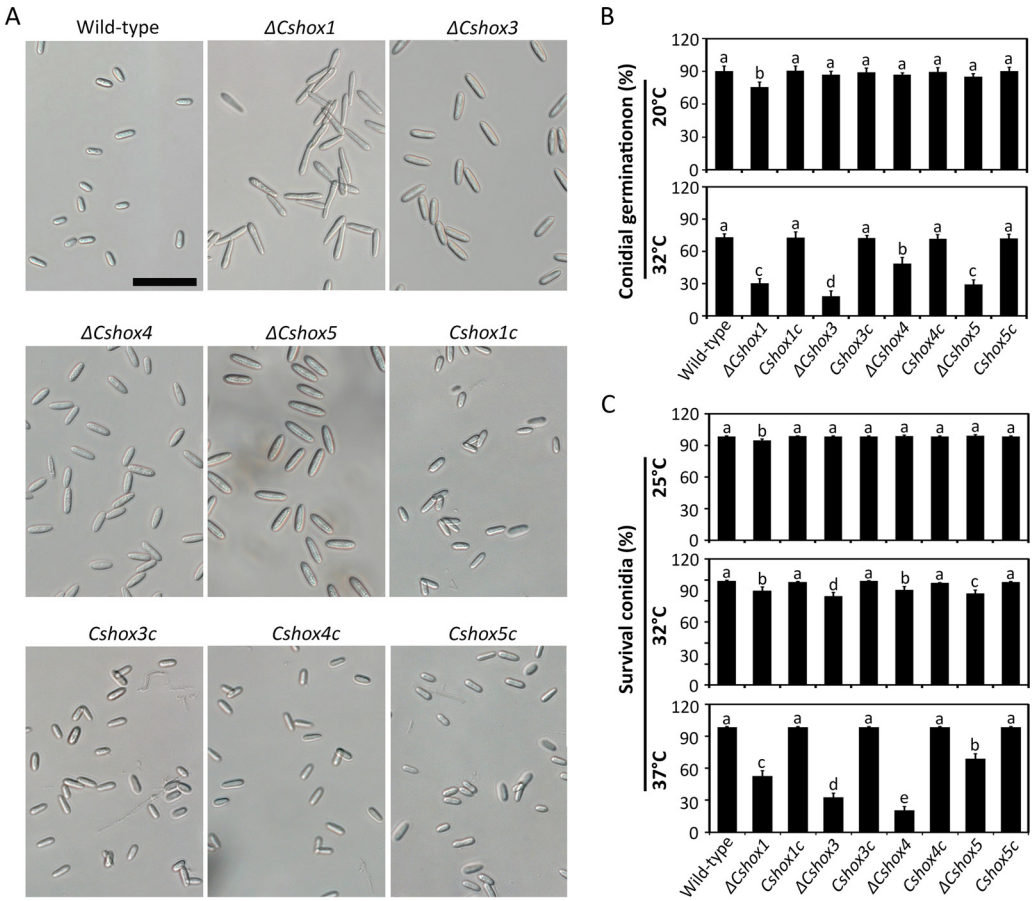


**FIG 2** *CsHOX1*, *CsHOX3*, *CsHOX4*, and *CsHOX5* are important for the morphology and germination of conidia and for stress response. (A) Observation of conidial morphology. Conidia were collected with $dH_2O$ from 7-day-old oatmeal agar. Scale bar, 25 $\mu$m. (B) Effects of temperature on conidial germination. Conidial suspensions ($5 \times 10^4$ ml$^{-1}$) were placed on hydrophobic coverslips and incubated in a humid box at 20°C and 32°C, which was controlled with respect to conidial germination at 25°C. (C) Effects of temperature on conidial longevities. Conidial suspensions ($10^7$ ml$^{-1}$) were placed at 25, 32, and 37°C for 16 h. Phloxine B (10 $\mu$g ml$^{-1}$) was used to test percentage of survival conidia. At least 100 conidia were evaluated each time. Significant differences were estimated by Duncan's test ($P < 0.05$). The same letter in a group with the same color indicates no significant difference.

32 or 37°C (Fig. 2C; see also Fig. S5D). These results suggested that *CsHOX1*, *CsHOX3*, *CsHOX4*, and *CsHOX5* are involved in conidial morphology, germination, and viability.

***CsHOX7* is required for appressorium development but not for invasive growth.** Appressorium development is a key step in anthracnose disease development in *C. scovillei*. Strikingly, conidia of the Δ*Cshox7* strain were completely abolished to produce appressoria, indicating that *CsHOX7* is essential for appressorium formation. A few swellings of the germ tube in the Δ*Cshox7* strain indicated that the Δ*Cshox7* strain retained the ability to sense the hydrophobic surface (Fig. 3A). Thus, we investigated the effects of exogenous chemical signals including cAMP, cutin monomers, and $CaCl_2$ on the recovery of appressorium development in the Δ*Cshox7* strain on hydrophobic coverslips. Conidia of the Δ*Cshox7* strain were unable to form appressoria with the addition of exogenous cutin monomers. However, cAMP (5 mM) induced formation of 24% immature appressoria in the Δ*Cshox7* strain, in contrast to 87.8% unmelanized appressoria in the wild-type strain (Fig. 3B and C). Compared to 91.5% formation of melanized appressoria by wild-type conidia, 44.5% of Δ*Cshox7* conidia developed young appressoria with the addition of $CaCl_2$ (0.5 mM) (Fig. 3B and C). These results revealed that exogenous cAMP or $CaCl_2$ partially restored appressorium formation in the Δ*Cshox7* strain. Treatment with both $CaCl_2$ and cAMP increased the appressorium formation rate of the Δ*Cshox7* strain to 82.8% and led to the formation of appressoria

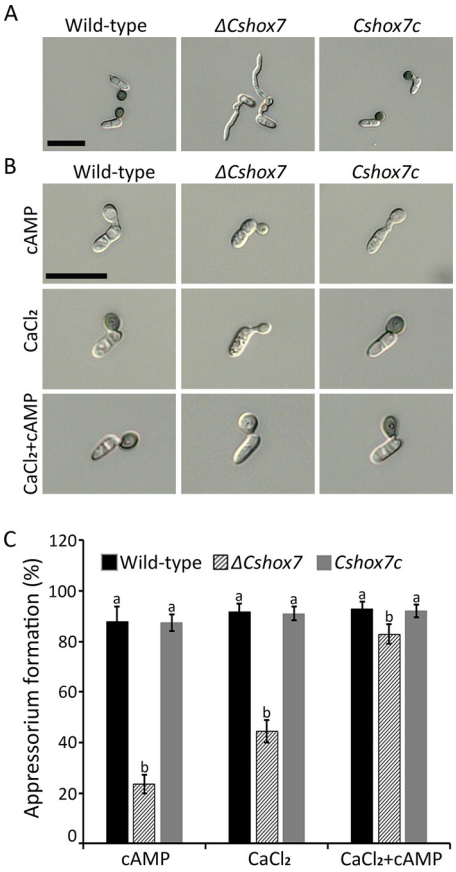


**FIG 3** *CsHOX7* is important for appressorium formation on a hydrophobic surface. (A) Appressorium formation. Conidial suspensions ($5 \times 10^4$ ml$^{-1}$) were placed on hydrophobic coverslips and incubated in a humid box at 25°C for 16 h. Scale bar, 20 $\mu$m. (B) Appressorium formation with exogenous 5 mM cAMP and 500 $\mu$M $CaCl_2$ or with 5 mM cAMP and 500 $\mu$M $CaCl_2$. Conidial suspension ($5 \times 10^4$ ml$^{-1}$) was dropped onto hydrophobic coverslips and incubated in a humid box at 25°C for 16 h. $CaCl_2$ and cAMP were added to the conidial suspension after 0 and 10 h, respectively. Scale bar, 20 $\mu$m. (C) Quantitative measurements of appressorium formation with addition of exogenous 5 mM cAMP and 500 $\mu$M $CaCl_2$ or of 5 mM cAMP and 500 $\mu$M $CaCl_2$. Appressorium formation rates were measured after 16 h on hydrophobic coverslips. Significant differences were estimated by Duncan's test ($P < 0.05$). The same letter in a group indicates no significant difference.

by 92.6% of wild-type conidia (Fig. 3C). Although appressoria of the Δ*Cshox7* strain induced by treatment with cAMP and $CaCl_2$ were not melanized, the sizes of appressoria were similar to those in the wild-type and *Cshox7c* strains (Fig. 3B). These compounds largely induced appressorium formation in the Δ*Cshox7* strain, suggesting that *CsHOX7* is regulated by cAMP and $Ca^{2+}$-dependent signaling pathways.

Compared to the wild-type strain, the Δ*Cshox7* strain caused full infection of wounded pepper fruit but produced no lesions on unwounded pepper fruit, revealing that the Δ*Cshox7* strain was unable to penetrate the host surface (Fig. 4A and B). Microscopic observation showed that conidia of the Δ*Cshox7* strain formed swollen structures at the tips of germ tubes that failed to differentiate into appressoria on the host surface (Fig. 4C). Because exogenous addition of $CaCl_2$ and cAMP partially restored appressorium formation in the Δ*Cshox7* strain on hydrophobic coverslips (Fig. 3B and C), we tested whether exogenous $CaCl_2$ and cAMP contributed to appressorium-mediated penetration of Δ*Cshox7*. Exogenous cAMP failed to restore infection by the Δ*Cshox7* strain (see Fig. S6A). However, conidia of the Δ*Cshox7* strain successfully infected unwounded pepper fruits with the addition of exogenous $CaCl_2$ (Fig. 4D and E). Treatment with both $CaCl_2$ and cAMP facilitated the formation of lesions by the Δ*Cshox7* strain on unwounded pepper fruits (Fig. 4D and E). Microscopic observation

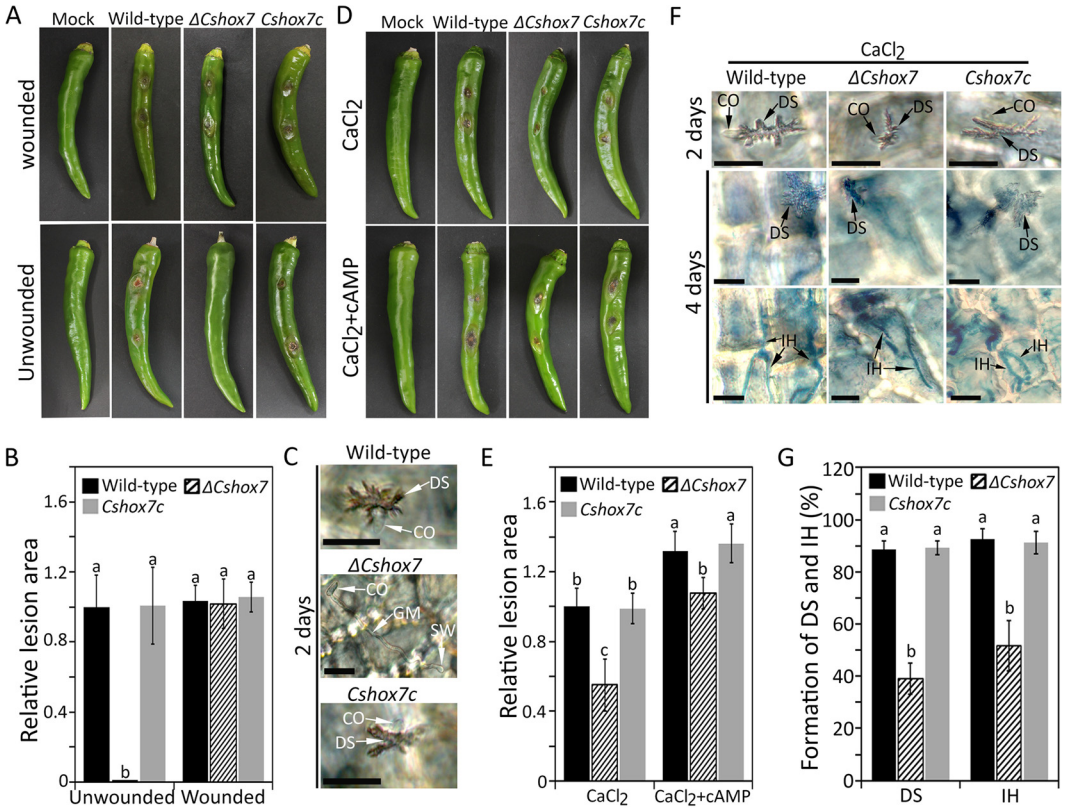


**FIG 4** *CsHOX7* is required for appressorium-mediated penetration. (A) Conidium-mediated infection assay on pepper fruits. Healthy wounded and unwounded pepper fruits were inoculated with conidial suspensions ($10^6$ ml$^{-1}$) and placed in a humid box at 25°C. Photographs were taken after 6 days for wounded assays and after 9 days for unwounded assays. (B) Quantitative analysis of lesion area. The lesion area was measured by using ImageJ and normalized to the lesion caused by the wild-type in unwounded pepper fruit as a relative of 1. (C) Appressorium penetration on pepper fruits. Unwounded pepper fruits were inoculated with conidial suspensions ($5 \times 10^4$ ml$^{-1}$) of indicated strains and placed in a humid box at 25°C for 2 days. Scale bar, 20 $\mu$m. (D) Recovery of conidium-mediated infection on pepper fruits. Unwounded pepper fruits were inoculated with conidial suspensions ($10^6$ ml$^{-1}$); 500 $\mu$M $CaCl_2$ or 500 $\mu$M $CaCl_2$/5 mM cAMP was then added. Photographs were taken after 9 days. (E) Quantitative analysis of relative lesion area. The lesion area was measured by using ImageJ and normalized to the lesion caused by the wild-type with exogenous addition of $CaCl_2$ as a relative of 1. (F) Recovery of appressorium penetration on pepper fruits. Unwounded pepper fruits were inoculated with conidial suspensions ($5 \times 10^4$ ml$^{-1}$) after the addition of 500 $\mu$M $CaCl_2$. Dendroid structures and invasive hyphae (blue) were observed after 2 and 4 days, respectively. Microscopic images with differently focused layers of the same samples for visualization of dendroid structure (upper panel) and invasive hyphae (lower) are shown. Scale bar, 20 $\mu$m. (G) Quantitative analysis of dendroid structure formation and invasive hyphae growth. The percentage of dendroid structure (DS) formation was evaluated by examining at least 100 conidia and calculating the proportion of conidia that induced DS in host tissue. The percentage of invasive hyphae was evaluated by examining at least 100 DS and calculating the proportion of DS, from which the invasive hyphae grew into at least one adjacent host cell. CO, DS, and IH indicate the conidium, dendroid structure, and invasive hyphae, respectively. Significant differences were estimated by Duncan's test ($P < 0.05$). The same letter in a group indicates no significant difference.

showed that the Δ*Cshox7* strain was partially restored to form dendroid structure and grow invasive hyphae in unwounded pepper fruit with an addition of exogenous $CaCl_2$ (Fig. 4F and G).

***CsHOX1* gene plays crucial roles in the development of anthracnose on pepper fruits.** The Δ*Cshox1* strain failed to infect wounded pepper fruit and led to charcoal-colored spots without typical sunken lesions on unwounded pepper fruit, which is not a typical disease symptom (Fig. 5A and B). To figure out the roles of *CsHOX1* in development of anthracnose on pepper fruits, we performed microscopic observation and found that the Δ*Cshox1* strain developed appressorium and penetrated the host surface, in a manner similar to that of wild-type and *Cshox1c* strains (Fig. 5C and D). Notably, in contrast to the wild-type and *Cshox1c* strains which grew invasive hyphae in host epidermal cells after 4 days, the host cells infected with the Δ*Cshox1* strain exhibited no invasive growth (Fig. 5C and D). We further investigated the expression

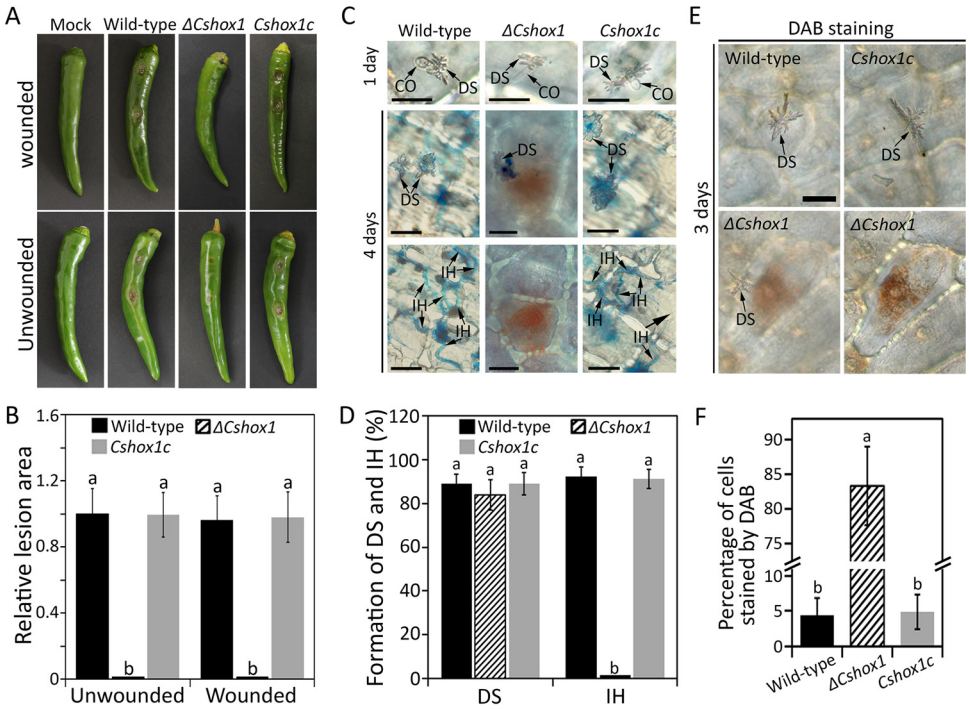


**FIG 5** *CsHOX1* is required for invasive hyphae growth. (A) Conidium-mediated infection assay on pepper fruits. Healthy wounded and unwounded pepper fruits were inoculated with conidial suspensions ($10^6$ ml$^{-1}$) and placed in a humid box at 25°C. Photographs were taken after 6 days for wounded assays and after 9 days for unwounded assays. (B) Quantitative analysis of lesion area. The lesion area was measured by using ImageJ and was normalized to the lesion caused by the wild-type in unwounded pepper fruit as a relative of 1. (C) Appressorium penetration of on pepper fruits. Unwounded pepper fruits were inoculated with conidial suspensions ($5 \times 10^4$ ml$^{-1}$) and placed in a humid box at 25°C. Dendroid structures were induced in the cuticle layer of pepper fruits after 1 day. Microscopic images with differently focused layers of the same samples for visualization of dendroid structure (upper panel) and invasive hyphae (lower) are shown. Scale bar, 20 $\mu$m. (D) Quantitative analysis of dendroid structure formation and invasive hyphae growth. The percentage of dendroid structure (DS) was evaluated by examining at least 100 conidia and calculating the proportion of conidia that induced DS in host tissue. The percentage of invasive hyphae was evaluated by examining at least 100 DSs and calculating the proportion of DSs, from which the invasive hyphae grew into at least one adjacent host cell. (E) Detection of ROS in the first host cell after 3 days. Accumulation of $H_2O_2$ was observed only in the first pepper cell challenged by the Δ*Cshox1* strain. Scale bar, 20 $\mu$m. (F) Quantitative analysis of $H_2O_2$ accumulation. The $H_2O_2$ accumulation was estimated by examining at least 100 DSs and calculating the proportion of DS, which induced ROS accumulation (stained by DAB) in at least one adjacent host cell. CO, DS, and IH indicate conidium, dendroid structure, and invasive hyphae, respectively. Significant differences were estimated by Duncan's test ($P < 0.05$). The same letter in a group indicates no significant difference.

profile of *CsHOX1* with qRT-PCR and found that the *CsHOX1* gene was highly expressed in infection stage (see Fig. S6B). These findings suggested that *CsHOX1* is essential for invasive hypha development during anthracnose development on pepper fruits.

The host cells infected by the Δ*Cshox1* strain exhibited brown pigmentation, which may reflect host cell defense response (59). Since host defense response is often accompanied by the rapid generation of reactive oxygen species (ROS), we performed the DAB staining experiment and found that pepper fruit cells infected with the Δ*Cshox1* strain exhibited a high density of $H_2O_2$ accumulation in the first challenged epidermal cell, whereas host cells infected with wild-type and *Cshox1c* strains did not show accumulation of $H_2O_2$ (Fig. 5E and F; see also Fig. S6C). To test whether *CsHOX1* is involved in the degradation of ROS, we evaluated the mycelial growth rate on CMA containing $H_2O_2$. Mycelial growth of the Δ*Cshox1* strain was significantly inhibited by 5 and 10 mM $H_2O_2$, and the Δ*Cshox1* strain was unable to grow on CMA containing 20 mM $H_2O_2$, whereas wild-type and *Cshox1c* strains could grow on this artificial media (Fig. 6A and B), suggesting that *CsHOX1* is required for degrading of ROS. We further evaluated the expression of host defense-related genes and found that *CaBPR1*, *CaPR4c*, *CaPR10*, *CaHIR1*, *CaGLP1*, *CaPIK1*, and *CaPAL1* were significantly upregulated in pepper

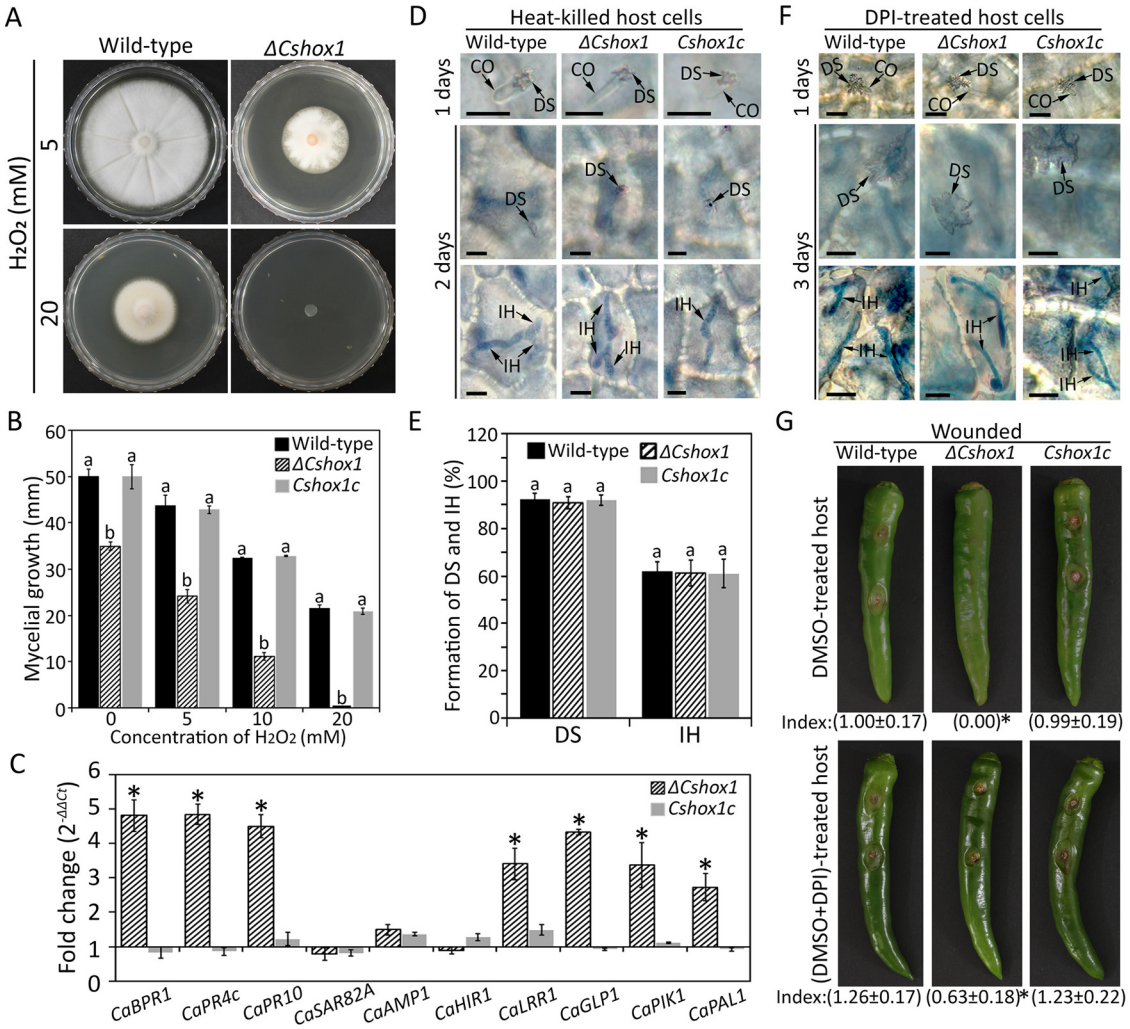


**FIG 6** *CsHOX1* is involved in suppression of host resistance. (A) Photographs of mycelial growth on CMA containing 0, 5, 10, and 20 mM $H_2O_2$. The mycelia were grown without light for 6 days. (B) Quantitative analysis of mycelial growth. Growth rate of mycelia was evaluated by measurement of diameter of colony growth after 6 days. (C) Expression of host defense-related genes in pepper fruit tissues infected with the Δ*Cshox1* strain, compared to tissues infected with the wild-type strain. qRT-PCR was performed, and the pepper actin gene was used as a reference. An asterisk (*) indicates a significant difference. (D) Observation of infection in heat-killed host tissues. The segments sliced from healthy pepper fruits were heated in boiling water for 30 s and then inoculated with conidial suspensions. The dendroid structure (DS) and invasive hyphae (IH) were observed at 1 and 3 days, respectively. Scale bar, 10 $\mu$m. (E) Quantitative analysis of DS and IH in heat-killed host tissues. The percentage of DS was evaluated by examining at least 100 conidia and calculating the proportion of conidia that induced DS in host tissue. The percentage of IH was evaluated by examining at least 100 DSs and calculating the proportion of DSs, from which the invasive hyphae grew into at least one adjacent host cell. (F) Observation of invasive growth in diphenyleneiodonium (DPI, suppressing ROS generation)-treated host tissues. The pepper fruits were first injected with DMSO containing DPI (2.5 $\mu$M) and then inoculated with conidial suspensions after 12 h. The dendroid structure and invasive hyphae were observed after 1 and 3 days, respectively. Scale bar, 10 $\mu$m. (G) Pathogenicity on DPI-treated pepper fruits. The wounded pepper fruits were drooped with 20 $\mu$l of DMSO (control) and 20 $\mu$l of DMSO containing DPI (2.5 $\mu$M) and inoculated with conidial suspensions after 12 h. Photographs were taken after 6 days. The index below each photo was the quantitative analysis of relative lesion area, and an asterisk (*) following the index of lesion area indicates a significant difference. The lesion area was measured by using ImageJ and was normalized to the lesion caused by the wild-type strain in DMSO-treated pepper fruits as a relative of 1. CO, DS, and IH indicate conidium, dendroid structure, and invasive hyphae, respectively. Significant differences were estimated by Duncan's test ($P < 0.05$). The same letter in a group with the same color indicates no significant difference.

fruits infected by the Δ*Cshox1* strain, compared to those infected by wild-type or *Cshox1c* strains (Fig. 6C; see also Table S2). This result indicated that CsHOX1 may be involved in suppression of host defense. Consistent with this hypothesis, we investigated the infection of the Δ*Cshox1* strain in defense-compromised host plant by inoculating conidial suspensions onto diphenyleneiodonium (DPI; suppressing ROS generation)-treated and heat-killed pepper fruits. The results showed that the invasive growth of the

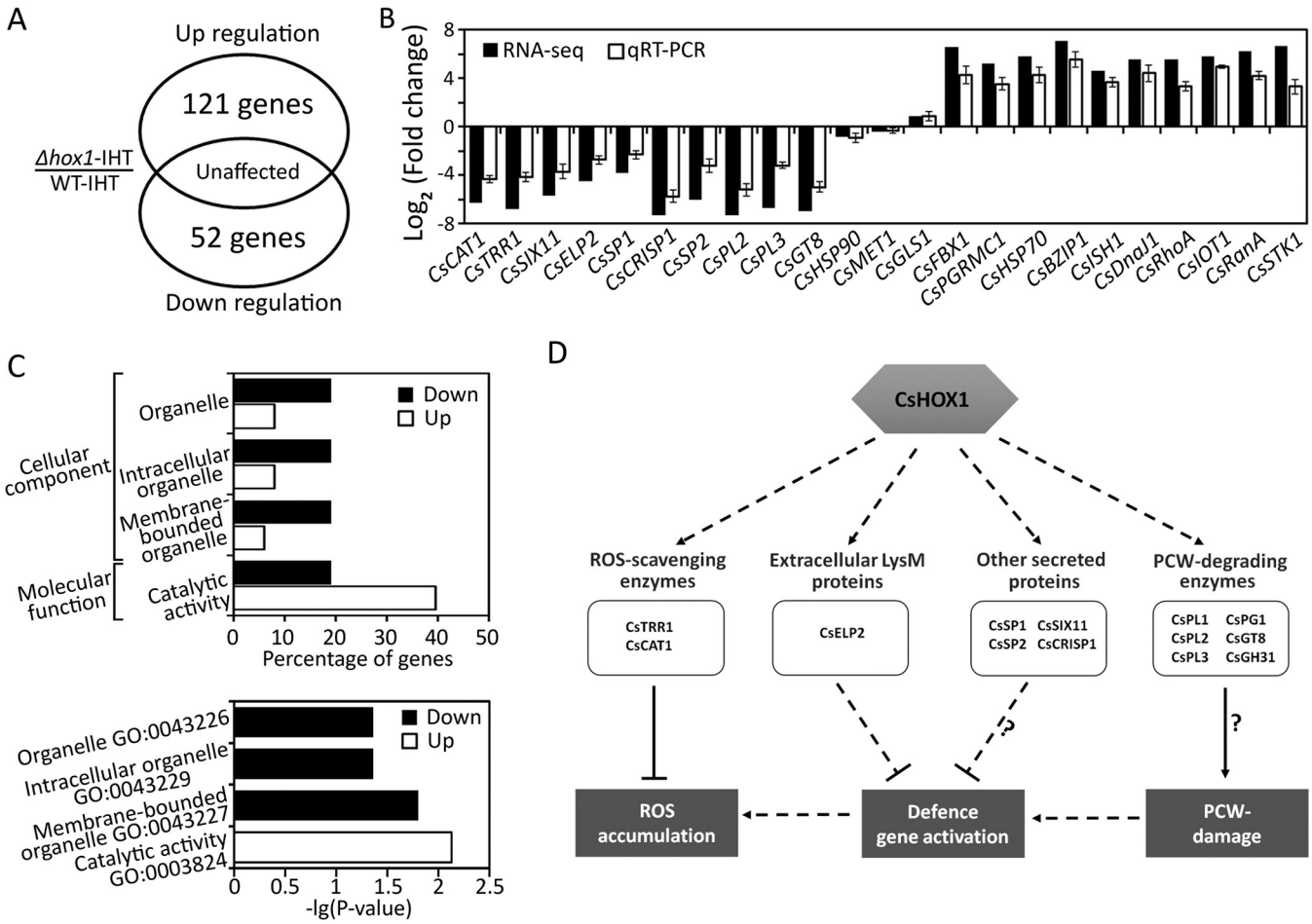


**FIG 7** Analysis of CsHOX1-dependent genes and hypothetical model of pathogenicity-related genes regulated by CsHOX1 in *C. scovillei*. (A) Venn diagram showing the number of differentially expressed genes (DEGs) from Δ*Cshox1* strain-infecting host tissues (Δ*Cshox1*-IHT) and wild-type strain-infecting host tissues (WT-IHT). The RNA-seq was performed with three biological replicates, and the DEGs were identified using the criterion with a false discovery rate of $<0.05$ and a $\log_2$(fold change) of $>2$. (B) Validation of RNA-seq results by using qRT-PCR. The selected genes for qRT-PCR included 10 upregulated, 10 downregulated, and 3 unaffected genes. The information of selected genes was shown in the Table S3B. (C) The Gene Ontology (GO) classification of upregulated and downregulated genes from RNA-seq. The main GO categories include cellular component and molecular function. (D) Hypothetical model of pathogenicity-related genes regulated by CsHOX1 in *C. scovillei*, based on the downregulated DEGs of Δ*Cshox1* strain-infecting host tissues (Δ*Cshox1*-IHT). Deletion of *CsHOX1* caused induction of host defense, including defense gene activation and ROS induction. Among the downregulated DEGs of Δ*Cshox1*-infecting tissues, CsTRR1 and CsCAT1 encode ROS-scavenging enzymes. CsELP2 encodes an extracellular LysM protein, which by suppresses the chitin-triggered immunity. Moreover, the genes encoding plant cell wall (PCW)-degrading enzymes (CsPL1, CsPL2, CsPL3, CsPG1, CsGT8, and CsGH31), significantly downregulated in the CsHOX1 deletion mutant, may cause PCW damage, thus triggering host defense. The four secreted proteins (CsSP1, CsSP2, CsSIX11, and CsCRISP1) may suppress the host defense, which remains further investigation. The information of all genes in the hypothetical model was shown in the Table S3C.

Δ*Cshox1* strain was comparable to that of wild-type and *Cshox1c* strains in heat-killed pepper fruits, and the infection of the Δ*Cshox1* strain was partially rescued in in DPI-treated pepper fruits (Fig. 6D to G). Taken together, these findings suggested that *CsHOX1* is involved in the degrading of ROS and the suppression of host defense.

***CsHOX1* regulates the expression of putative virulence-related genes.** To further investigate the *CsHOX1*-dependent genes during anthracnose development in pepper fruits, we performed the RNA-seq to profile the gene expression of host tissues infected by the Δ*Cshox1* strain versus the wild-type strain. The result showed that 52 genes were significantly downregulated ($\log_2$-fold change, $<-2$; $P < 0.05$), and 121 genes were significantly upregulated ($\log_2$-fold change, $>2$; $P < 0.05$) in host tissues infected by the Δ*Cshox1* strain in reference to the wild-type strain (Fig. 7A; see also Table S3A). To validate the RNA-seq result, we evaluated the 10 upregulated differentially expressed genes (DEGs), 10 downregulated DEGs, and 3 unaffected genes to evaluate their expression with qRT-PCR (Fig. 7B). The expression of 10 selected upregulated genes, encoding

putative pathogenicity-related secreted proteins, ROS-scavenging enzymes, and plant cell wall-degrading enzymes (see Table S3B), was consistent with that obtained from RNA-seq. The transcripts of 10 selected downregulated genes, involved in stress response and signal transduction (see Table S3B), were also similar to that from RNA-seq. The Gene Ontology (GO) term enrichment test showed that none of the functions in downregulated genes enriched compared to the whole gene sets, but the upregulated genes were enriched with functions involved in many cellular components, bindings, and metabolic processes (see Fig. S6D). The enrichment test between down- and upregulated genes showed genes related to organelles in the cellular component category were enriched in the downregulated genes, and genes with catalytic activity were enriched in upregulated genes (Fig. 7C). This result indicates that *CsHOX1* may play an important role in regulation of genes associated with the organelle formation and the catalytic activities. Further analysis of downregulated genes revealed that 13 genes were putative pathogenicity factors, including two ROS-scavenging enzymes (60, 61), five secreted proteins (62), and six plant cell wall-degrading enzymes (see Table S3C) (63). Many genes were upregulated in the Δ*Cshox1* strain, including regulators such as protein kinases, phosphatases, and transcription factors. The RNA-seq data supported that the *CsHOX1* plays a key role in regulating anthracnose development of *C. scovillei* on pepper fruits.

## DISCUSSION

TFs play critical roles in development and pathogenicity in organisms, including fungal pathogens. Essential functions of the evolutionarily conserved homeobox TFs have been demonstrated in several eukaryotes (35, 64). In this study, analysis of TFomes and homeodomain superfamily genes in *C. scovillei* was extended to the *Colletotrichum* species complex and selected outgroup species. These analyses revealed that *C. scovillei* has a unique feature within the *Colletotrichum* species complex; notably, the fungus exhibited an extremely high number of homeodomain superfamily genes, while *HOX* genes were evenly distributed among the species complex (Fig. 1A). In terms of InterPro domain relationships, the homeobox-like domain superfamily (IPR009057) is one of the largest gene families in the kingdom Fungi, inclusive of the homeobox domain (IPR001356) in *HOX* genes (40). This duplication event was observed in both *C. scovillei* and *S. sclerotiorum*, an outgroup species (Fig. 1A); this shared feature was attributed to the DNA transposon TcMar-Fot1 (Fig. 2A). While the expansion and enrichment of DNA transposons in the genome of *S. sclerotiorum* have been reported (65), the relationships of DNA transposons with the duplication of homeodomain superfamily genes are first reported here for both *S. sclerotiorum* and *C. scovillei*. Unlike tandem clusters of *HOX* genes in animals, *HOX* genes were found to be scattered throughout the genomes of fungi, including *C. scovillei* (Fig. 2B) (66). However, these homeobox-like genes were revealed to be duplicated multicopy genes located in a tandem manner in the *C. scovillei* genome (Fig. 2B). This is likely evidence for the recent transposon activity that occurred in *C. scovillei* after divergence from *C. nymphaeae* (see Fig. S1A), which presumably occurred approximately 2 million years ago (57, 67). Because transposable elements are the major drivers of fungal genome evolution (68), the association of transposons with homeodomain superfamily genes impacts genome organization and may affect cellular processes related to fungal development and pathogenicity.

Molecular mechanisms that govern anthracnose disease caused by *Colletotrichum* species on fruits have not yet been characterized. A large number of conidia are reproduced from phialides of conidiophores in many *Colletotrichum* species (69, 70). However, the genetic basis of the conidiation process remains largely unknown in the *Colletotrichum* genus. We found that the deletion of *CsHOX2* caused a complete defect in the production of conidia in *C. scovillei*, whereas the Δ*Cshox2* strain developed normal conidiophores (Fig. 3). Considering that *MoHOX2* (orthologous to *CsHOX2*) is essential for *M. oryzae* conidiation in a stage-specific manner (33), the development of phialides on top of conidiophores, which are not clearly distinguishable, may be normal in the Δ*Cshox2* strain. However, *HTF1* genes in *Fusarium graminearum*, *F. verticillioides*,

and *F. oxysporum* (all orthologous to *CsHOX2*) were revealed to be involved in the formation of clearly differentiated phialides (50). The Δ*Fghtf1*, Δ*Fvhtf1*, and Δ*Fohtf1* strains alternatively produce macroconidia directly from hyphae at low frequencies, indicating functional differences in *CsHOX2* from orthologous *HTF1* genes in the three *Fusarium* species. Unlike the complete defect of the Δ*Cshox2* strain in conidium production, it is notable that the deletions of *CsHOX1*, *CsHOX3*, *CsHOX4*, and *CsHOX5* resulted in the development of abnormally large conidia (Fig. 4A); in contrast, deletion of *MoHOX4* (orthologous to *CsHOX4*) resulted in the production of abnormally small conidia in *M. oryzae* (33). Notably, 4 of 10 *HOX* genes are associated with conidial size and morphology in *C. scovillei*. Several lines of evidence suggest that the four genes play distinct roles in conidium development of *C. scovillei*. For example, the Δ*Cshox1* strain produced significantly larger conidia (19.9 ± 2.4 $\mu$m) compared to those from the Δ*Cshox3*, Δ*Cshox4*, and Δ*Cshox5* strains (3.4 ± 0.3 $\mu$m, 15.0 ± 1.7 $\mu$m, and 4.2 ± 0.5 $\mu$m) (Table 1). Abnormal swelling of the conidia and germ tubes was observed in Δ*Cshox1* alone (not in the Δ*Cshox3*, Δ*Cshox4*, and Δ*Cshox5* strains), following treatment with nikkomycin Z; this indicated a difference in cell wall integrity (see Fig. S4B). The sensitivity of conidia in the Δ*Cshox3* strain was much higher following treatment with the fungicide carbendazim, compared to the sensitivities of conidia in the Δ*Cshox1*, Δ*Cshox4*, and Δ*Cshox5* strains (see Fig. S4A), which support functional differences among the four *CsHOX* genes in *C. scovillei.* The *CsHOX1* gene is a critical regulator of cell wall integrity and conidia morphology, as well as pathogenic development, in *C. scovillei* (Fig. 4A and 7E; see also Fig. S4B), which represents a novel function of homeobox TFs in plant-pathogenic fungi.

The Δ*Cshox1* strain was not defective in appressorium formation and host penetration on pepper fruits (Fig. 5C and D). The invasive hyphae of the Δ*Cshox1* strain were unable to grow in the epidermal cells of pepper, following successful penetration into the cuticle layer via appressoria (Fig. 5C). The accumulation of the brown cloud and ROS only in the first epidermal cell challenged by the Δ*Cshox1* mutant (Fig. 5E and F), and the significant upregulation of host defense-related genes were indicative of the activation of innate host immunity (Fig. 6C; see also Table S2). The increased sensitivity of the Δ*Cshox1* mutant to $H_2O_2$, compared to the wild-type and *Cshox1c* strains, indicates that *CsHOX1*-regulated genes may be related to the modulation of ROS that are encountered in host pepper cells during anthracnose development of *C. scovillei* (Fig. 6A and B). Notably, the ROS-scavenging enzymes CsTRR1 and CsCAT1, orthologous to *M. oryzae* TRR1 and *Sclerotinia sclerotiorum* SCAT1, respectively, were significantly downregulated in gene expression profiles (see Table S3C). Both TRR1 and SCAT1 were reported to play important roles in ROS detoxification and plant infection (60, 61). The significant downregulation of *CsTRR1* and *CsCAT1* in Δ*Cshox1*-infecting host tissues revealed the involvement of *CsHOX1* in ROS detoxification. Moreover, an LysM protein CsELP2, orthologous to *C. higginsianum* ChELP2, were found in the significantly downregulated genes (Fig. 7B). The ChELP2 encodes an extracellular LysM protein, which suppresses chitin-triggered plant immunity (71). The fungal chitin is known to induce host ROS accumulation and defense gene activation (72). This suggests that the CsHOX1 may be involved in suppression of chitin triggered immunity through transcriptional regulation of CsELP2. When performing pathogenicity assay by using host defense-comprised tissues, the Δ*Cshox1* could grow invasive hyphae as wild-type strain did on heat-killed host tissues (Fig. 6D and E), while the pathogenicity was partially restored on DPI-treated host (Fig. 6F and G). This result indicated that the CsHOX1-regulated genes may be involved in suppression of host defense. In addition, the other four genes encoding secreted proteins (CsSIX11, CsCRISP1, CsSP1, and CsSP2) were found to be significantly downregulated in Δ*Cshox1* strain-infected host tissues (Fig. 7B). The CsSIX11 was predicted to be orthologs to a known effector, SIX11 (Secretion In Xylem) of *Fusarium oxysporum*, which was recently demonstrated to be dispensable for fungal virulence, while its role in host defense is still unknown (73). The *CsCRISP1* gene was predicted to encode a cysteine-rich secretory protein. Although the

ortholog of CsCRISP1 was not characterized, the cysteine-rich secretory proteins were reported to be involved in suppression of plant immunity in *Verticillium dahliae* (74). The detailed mechanisms of CsSIX11 and CsCRISP1 await investigation. These findings suggested that CsHOX1 is an essential factor that contributes to anthracnose development by transcriptional regulation of genes involved in the modulation of ROS and host defense (Fig. 7D).

Our study of appressorium-mediated fruit disease development in *C. scovillei* demonstrated that it uses a different strategy, compared to other fungal pathogens, to effectively penetrate the thick cuticle layer (20 to 25 $\mu$m) of host cells. For example, *M. oryzae*, a model for foliar disease in rice, generates substantial turgor pressure inside the appressorium to directly reach invading epidermal cells through the host cell wall by means of a strong mechanical force (75). However, *C. scovillei* has evolved a highly sophisticated strategy in which the fungus achieves tiny pin-point entry via the appressorium and then grows in the thick cuticle layer with the formation of dendroid structures within the cuticle layer; it does not use a penetration peg (2 to 4 $\mu$m in length) that directly reaches the epidermal cells of the pepper fruit. Therefore, *C. scovillei* generates, possibly, lower turgor pressure inside the appressorium and maintains conidial viability after penetration, in contrast to the autophagic cell death of conidia that occurs following penetration of *M. oryzae* (76). This hypothesis is supported by the observation that unpigmented immature appressoria of *C. scovillei* are able to penetrate the cell wall of pepper fruit and cause anthracnose disease (data not shown).

In this study, we demonstrated the dynamics and proliferation of homeodomain superfamily TFs during the evolution of an ingroup of *Colletotrichum* species and outgroup members. Detailed functional analyses have revealed that members of the homeobox TF family in *C. scovillei* play a key role in fungal development and anthracnose disease on pepper fruit. Our study provides a fundamental basis for understanding the molecular mechanisms involved in conidiation, appressorium development, and anthracnose disease on fruits, which will contribute to the development of novel strategies for use in managing anthracnose disease on many economically important fruits.

## MATERIALS AND METHODS

**Data used in the study and prediction of TFomes and repeat elements.** The fungal genomes and proteomes used in this study were downloaded from the National Center for Biotechnology Information (NCBI) database (see Table S1A). TFs were identified from proteomes using InterProScan 5.35-74, based on previously reported fungal TFs (40). Repeat elements were annotated using RepeatMasker 4.0.9 with a fungal repeat library (20170127) from RepBase (77).

**Identification of genes influenced by *HOX* genes in *C. scovillei*.** *HOX* genes of *C. scovillei*, *M. oryzae*, and *Saccharomyces cerevisiae* and their domains were aligned using MAFFT 7.29 (78); their sequence identities were calculated using the sident program in the trimAl v1.2 package (79). The binding domains of yeast *HOX* genes (YHP1, YOX1, TOS8, and CUP9) were retrieved from the JASPAR2020 database and used to search potential binding sites in the genome of *C. scovillei* (80). The binding sites were identified by PWMScan using the repeat masked intergenic sequences of the genome (81). Genes within 2 kb downstream of binding sites were collected; level 3 Gene Ontology term functions were visualized using WEGO (20181101) (82).

**Fungal strains and culture conditions.** *C. scovillei* strain KC05, originally isolated from pepper (*C. annuum*) in Gangwon Province, South Korea (32), was used as the wild-type strain. The strain and its transformants were routinely grown on V8 agar medium (80 ml liter$^{-1}$ V8 juice and 15 g liter$^{-1}$ agar powder), potato dextrose agar medium (39 g liter$^{-1}$ powder; Kisan Bio, Seoul, South Korea), or oatmeal agar (50 g liter$^{-1}$ oatmeal and 15 g liter$^{-1}$ agar powder) with fluorescent light at 25°C (83). Mycelia for DNA or RNA extraction were cultured in liquid complete medium (CM; 6 g liter$^{-1}$ yeast extract, 6 g liter$^{-1}$ Casamino Acids, and 10 g liter$^{-1}$ sucrose) or on TB3 agar medium (200 g liter$^{-1}$ sucrose, 10 g liter$^{-1}$ glucose, 3 g liter$^{-1}$ yeast extract, 3 g liter$^{-1}$ Casamino Acids, and 8 g liter$^{-1}$ agar powder).

**Localization of histone H1:DsRed and CsHOX:sGFP fusion protein.** The histone H1:DsRed and CsHOX:sGFP fusion vectors were constructed by overlap cloning method (84, 85). PCR product of histone H1 (1.1 kb) was amplified with paired primers CAP_006988_F/CAP_006988_R (see Table S4), from wild-type genomic DNA. Also, 5.6 kb of DsRed fragment containing *HPH* gene and promoter of *Neurospora crassa* isocitrate lyase (ICL) encoding gene was amplified with the primer pair pIG-006988_F/pIG-006988_R from pIGPAPA-DsRed (84). The histone H1 fragment and DsRed fragment were combined by using an overlap DNA cloning kit (Elpis Biotech, Daejeon, South Korea), in which DsRed is under the control of *Neurospora crassa ICL* promoter. The recombinant vector of histone H1:DsRed was transformed into wild-type protoplasts. *CsHOX* fragments containing 1.5 kb of the promoter region and ORF (open reading frame) minus stop codon of *CsHOX2* or *CsHOX7* genes was amplified with the paired primers

CAP_006569_F/CAP_006569_R or CAP_005766_F/CAP_005766_R from wild-type genomic DNA. As well, 5.0 kb of sGFP fragments including a Geneticin resistance gene was amplified with the paired primers pIG-006569_F/pIG-006569_R or pIG-005766_F/pIG-005766_R from pIGPAPA-sGFP (84). The *CsHOX* fragment and sGFP fragment were combined as described above, in which sGFP is fused to *CsHOX* and under the control of native *CsHOX* promoter. Each recombinant construct of CsHOX:sGFP was then transformed into protoplasts of transformants expressing histone H1:DsRed.

**Generation of deletion mutants and complemented transformants.** The targeted gene deletion vector was constructed based on a modified double-joint PCR (86). Briefly, the 1.5-kb region on upstream and downstream of target gene (*CsHOX1* to *CsHOX10*) was amplified with the paired primers 5F/5R and 3F/3R of each gene, respectively (see Table S4). The *hygromycin B phosphotransferase* (*HPH*) gene was amplified with the primers HPHF/HPHR and fused with 1.5-kb upstream and downstream regions of each *HOX* genes by rounds of fusion PCR (87, 88). The fused deletion construct was then amplified in a nested PCR with the paired primers NF/NR. The product from nested PCR was introduced into the wild-type protoplasts by a polyethylene glycol-mediated transformation method as previously described (32). All transformants were first selected by a screening PCR with the paired primers SF/SR and finally confirmed by Southern blotting and RT-PCR. For complementation, the paired primers NF/NR were used to amplify each *HOX* gene. The PCR product and a 1.5-kb Geneticin resistance cassette were then cointroduced into protoplasts of each deletion mutant for *CsHOX* genes. The transformants of complementation were verified by RT-PCR.

**Nucleic acid manipulation and gene expression.** Fungal genomic DNA was prepared according to a quick and safe extraction method for general screening PCR, or a standard extraction method for Southern blot analysis (89, 90). The 500-kb DNA segment used as the Southern blot probe was amplified with the paired primers PF/PR (see Table S4). The genomic DNA was digested with specific restriction enzyme and then probed with that 500-kb DNA segment, which was previously labeled with Biotin-High Prime (Roche, Indianapolis, IN). To perform qRT-PCR and RT-PCR, total RNA was isolated from frozen fungal tissues and infected plant tissues using an Easy-Spin Total RNA extraction kit (iNtRON Biotechnology, Seongnam, South Korea). The complementary DNA (cDNA) was reverse transcribed from 5 $\mu$g of total RNA using SuperScript III first-strand synthesis system for RT-PCR kit (Invitrogen, Carlsbad, CA). The qRT-PCR mixture (10 $\mu$l) contained 1 $\mu$l of cDNA template (25 ng/$\mu$l), 1 $\mu$l of forward primer qrtF, 1 $\mu$l of reverse primer qrtR, and 5 $\mu$l of real-time PCR 2× master mix (Elpis, Daejeon, South Korea). The qRT-PCR experiment was performed with two replicates in three independent experiments using the StepOne real-time PCR system (Applied Biosystems, Foster city, CA). The PCR was set as follows: 95°C for 3 min (1 cycle), followed by 95°C for 15 s, 58°C for 30 s, and 72°C for 30 s (40 cycles). To measure the relative transcript abundance, $C_T$ values were normalized to those of *β-tubulin* of *C. scovillei* or *Actin* of *C. annuum*. The normalized fold change of the target gene expression was expressed as $2^{-\Delta\Delta CT}$, where $-\Delta\Delta C_T = \Delta C_{T\,\text{control}} - \Delta C_{T\,\text{tested condition}}$ (91).

**Phenotypic characterization of mutants.** Vegetative growth of mycelium was evaluated by measuring the diameters of colonies grown on complete medium agar (CMA; 10 g liter$^{-1}$ sucrose, 6 g liter$^{-1}$ yeast extract, 6 g liter$^{-1}$ Casamino Acids, and 15 g liter$^{-1}$ agar powder) or minimal medium agar (MMA; 0.1 ml liter$^{-1}$ trace elements, 30 g liter$^{-1}$ sucrose, 2 g liter$^{-1}$ $NaNO_3$, 1 g liter$^{-1}$ $KH_2PO_4$, 0.5 g liter$^{-1}$ KCl, 0.5 g liter$^{-1}$ $MgSO_4{\cdot}7H_2O$, and 15 g liter$^{-1}$ agar powder). Conidiation was evaluated by counting conidia collected with 5 ml of distilled water from 7-day-old V8 agar. Lactophenol aniline blue solution was used to distinguish conidiophores from mycelia (33, 92). For conidial germination and appressorium formation, drops of conidial suspension (20 $\mu$l; $5 \times 10^4$ ml$^{-1}$) were placed on hydrophobic coverslips, then incubated in a humid box. The numbers of germinated conidia and conidia with appressoria were counted in a sample of 100 conidia. To evaluate germination of conidia subjected to chemical stress, the conidial suspension was placed on hydrophobic coverslips; the fungicides dimethomorph, oxolinic acid, carbendazim, and fludioxonil were added at concentrations of 1, 0.1, or 1 ppm. To test the germination of conidia subjected to temperature stress, the conidial suspension was placed on hydrophobic coverslips and incubated at 20, 25, or 30°C. The chitin synthase inhibitor nikkomycin Z was used to test the cell wall integrities of conidia and germ tubes. Dead conidia were stained and distinguished by phloxine B in a conidial viability assay. Exogenous $CaCl_2$ or cAMP was used to promote appressorium development. Data were collected from three independent experiments with at least three replicates per experiment. Significant differences were analyzed by Duncan's test ($P < 0.05$).

**Plant infection assays.** The wounded plant infection assay was performed by placing a conidial suspension ($10^6$ ml$^{-1}$) on wounded healthy pepper fruit, which were then incubated in a humid box for 9 days at 25°C. For the unwounded plant infection assay, the conidial suspension was placed on unwounded healthy pepper fruit, followed by incubation for 6 days at 25°C. To observe fungal invasive hyphae inside pepper cells, a modified trypan blue solution containing 0.05% trypan blue (wt/vol), 30% phenol B (vol/vol), and 30% lactic acid (vol/vol) was applied. Briefly, healthy pepper fruits were inoculated with conidial suspension ($5 \times 10^4$ ml$^{-1}$) and incubated for 4 days. The thin sections of infected pepper fruits were cut with a razor blade and fixed in a solution containing 10% (vol/vol) acetic acid, 30% (vol/vol) chloroform, and 60% (vol/vol) methanol for at least 16 h. The fixed samples were subsequently rehydrated in ethanol solutions of decreasing concentrations (100% [vol/vol], 70% [vol/vol], and 50% [vol/vol]) for at least 3 h at each concentration. The samples were then stained in modified trypan blue solution and destained with 70% (vol/vol) ethanol. The stained samples were embedded in 30% (vol/vol) glycerol and observed through a microscope. 3,3′-Diaminobenzidine (DAB) was used to stain hydrogen peroxide ($H_2O_2$) in pepper fruit cells. The thin sections of infected pepper fruits were infiltrated with DAB solution (1 mg ml$^{-1}$ [pH 7.5]) under vacuum and boiled in 96% (vol/vol) ethanol for 10 min (93). The

accumulation of iron ($Fe^{3+}$) in tissues of pepper fruits was indicated by Perls Prussian blue staining according to previously reported methods (94, 95).

**RNA-seq and differentially expressed gene analyses.** The healthy fruits (green color) of chili pepper (*Capsicum annuum*) inoculated with 20 $\mu$l of distilled water or a conidial suspension ($25 \times 10^4$ conidia/ml) of the wild-type or the Δ*Cshox1* strain were put in humid plastic boxes and incubated at 25°C for 48 h. The thin segments containing the outer cuticle layer, and epidermal cells were sliced from the infected pepper fruits with a razor blade. Each segment obtained from pepper fruit tissues was observed through a light microscope and confirmed to be infected by the wild-type or Δ*Cshox1* strain. The confirmed segments were subsequently immersed in the liquid nitrogen. Each RNA sample was extracted from 30 segments using the Easy-Spin total RNA extraction kit (Intron Biotechnology, Seongnam, South Korea) according to the manufacturer's instructions. The three biological replicates of extracted RNA samples were then sequenced by Illumina Hiseq 2500 (NICEM, Seoul, South Korea). The quality of raw read data from each sample was checked with fastp v0.21.0, including adaptor trimming and low-quality read filtering (96). The trimmed read data were mapped to the reference genome of *C. scovillei* using HISAT2 v2.2.1 (97), and the read count of reference genes was performed using StringTie2 v2.1.5 (98). The DEG analysis between the wild-type and Δ*Cshox1* strains was performed using DESeq2 (99).

**Data availability.** The transcriptome data of *C. scovillei* wild-type and Δ*Cshox1* strains were submitted to the SRA database in NCBI under accession numbers SRR13957602 to SRR13957604 and SRR13957605 to SRR13957607, respectively.

## SUPPLEMENTAL MATERIAL

Supplemental material is available online only.

**FIG S1**, TIF file, 2.7 MB.
**FIG S2**, TIF file, 2.2 MB.
**FIG S3**, TIF file, 2.8 MB.
**FIG S4**, TIF file, 1.8 MB.
**FIG S5**, TIF file, 1.5 MB.
**FIG S6**, TIF file, 1.6 MB.
**TABLE S1**, XLSX file, 0.2 MB.
**TABLE S2**, XLSX file, 0.01 MB.
**TABLE S3**, XLSX file, 0.04 MB.
**TABLE S4**, XLSX file, 0.02 MB.

## ACKNOWLEDGMENTS

This study was supported by Basic Science Research Program through the National Research Foundation of Korea grant (NRF-2020R1A2C100550700) funded by the Ministry of Education, Science and Technology, and by a grant (918019043HD020) from the Strategic Initiative for Microbiomes in Agriculture and Food, Ministry of Agriculture, Food and Rural Affairs, Republic of Korea. The funders had no role in study design, data collection and analysis, decision to publish, or preparation of the manuscript.

## REFERENCES

1. Kim S, Park M, Yeom S-I, Kim Y-M, Lee JM, Lee H-A, Seo E, Choi J, Cheong K, Kim K-T, Jung K, Lee G-W, Oh S-K, Bae C, Kim S-B, Lee H-Y, Kim S-Y, Kim M-S, Kang B-C, Jo YD, Yang H-B, Jeong H-J, Kang W-H, Kwon J-K, Shin C, Lim JY, Park JH, Huh JH, Kim J-S, Kim B-D, Cohen O, Paran I, Suh MC, Lee SB, Kim Y-K, Shin Y, Noh S-J, Park J, Seo YS, Kwon S-Y, Kim HA, Park JM, Kim H-J, Choi S-B, Bosland PW, Reeves G, Jo S-H, Lee B-W, Cho H-T, Choi H-S, et al. 2014. Genome sequence of the hot pepper provides insights into the evolution of pungency in *Capsicum* species. Nat Genet 46: 270–278. https://doi.org/10.1038/ng.2877.
2. FAOSTAT. 2018. Database: Food and Agriculture Organization of the United Nations–FAOSTAT. FAOSTAT, Rome, Italy. http://www.fao.org/faostat/en/#data/QC/visualize. Accessed 5 June 2020.
3. Förster H, Adaskaveg J. 1999. Identification of subpopulations of *Colletotrichum acutatum* and epidemiology of almond anthracnose in California. Phytopathology 89:1056–1065. https://doi.org/10.1094/PHYTO.1999.89.11.1056.
4. Saxena A, Raghuwanshi R, Gupta VK, Singh HB. 2016. Chilli anthracnose: the epidemiology and management. Front Microbiol 7:1527. https://doi.org/10.3389/fmicb.2016.01527.
5. Cannon P, Damm U, Johnston P, Weir B. 2012. *Colletotrichum*: current status and future directions. Stud Mycol 73:181–213. https://doi.org/10.3114/sim0014.
6. Kim K-H, Yoon J-B, Park H-G, Park EW, Kim YH. 2004. Structural modifications and programmed cell death of chili pepper fruit related to resistance responses to *Colletotrichum gloeosporioides* infection. Phytopathology 94:1295–1304. https://doi.org/10.1094/PHYTO.2004.94.12.1295.
7. Ranathunge N, Ford R, Taylor P. 2009. Development and optimization of sequence-tagged microsatellite site markers to detect genetic diversity within *Colletotrichum capsici*, a causal agent of chili pepper anthracnose disease. Mol Ecol Resour 9:1175–1179. https://doi.org/10.1111/j.1755-0998.2009.02608.x.
8. Han J-H, Chon J-K, Ahn J-H, Choi I-Y, Lee Y-H, Kim KS. 2016. Whole-genome sequence and genome annotation of *Colletotrichum acutatum*, causal agent of anthracnose in pepper plants in South Korea. Genom Data 8:45–46. https://doi.org/10.1016/j.gdata.2016.03.007.
9. Caires NP, Pinho DB, Souza JSC, Silva MA, Lisboa DO, Pereira OL, Furtado GQ. 2014. First report of anthracnose on pepper fruit caused by *Colletotrichum scovillei* in Brazil. Plant Dis 98:1437. https://doi.org/10.1094/PDIS-04-14-0426-PDN.
10. Kanto T, Uematsu S, Tsukamoto T, Moriwaki J, Yamagishi N, Usami T, Sato T. 2014. Anthracnose of sweet pepper caused by *Colletotrichum scovillei* in Japan. J Gen Plant Pathol 80:73–78. https://doi.org/10.1007/s10327-013-0496-9.
11. Zhao W, Wang T, Chen Q, Chi Y, Swe T, Qi R. 2016. First report of *Colletotrichum scovillei* causing anthracnose fruit rot on pepper in Anhui

Province, China. Plant Dis 100:2168–2168. https://doi.org/10.1094/PDIS-04-16-0443-PDN.
12. Oo MM, Lim G, Jang HA, Oh S-K. 2017. Characterization and pathogenicity of new record of anthracnose on various chili varieties caused by *Colletotrichum scovillei* in Korea. Mycobiology 45:184–191. https://doi.org/10.5941/MYCO.2017.45.3.184.
13. Noor NM, Zakaria L. 2018. Identification and characterization of *Colletotrichum* spp. associated with chili anthracnose in peninsular Malaysia. Eur J Plant Pathol 151:961–973. https://doi.org/10.1007/s10658-018-1431-x.
14. de Silva DD, Groenewald JZ, Crous PW, Ades PK, Nasruddin A, Mongkolporn O, Taylor PWJ. 2019. Identification, prevalence and pathogenicity of *Colletotrichum* species causing anthracnose of *Capsicum annuum* in Asia. IMA Fungus 10:8–32. https://doi.org/10.1186/s43008-019-0001-y.
15. Khalimi K, Darmadi AAK, Suprapta DN. 2019. First report on the prevalence of *Colletotrichum scovillei* associated with anthracnose on chili pepper in Bali, Indonesia. Int J Agric Biol 22:363–368.
16. Zhou Y, Huang J, Yang L, Wang G, Li J. 2017. First report of banana anthracnose caused by *Colletotrichum scovillei* in China. Plant Dis 101:381. https://doi.org/10.1094/PDIS-08-16-1135-PDN.
17. Qin LP, Zhang Y, Su Q, Chen YL, Nong Q, Xie L, Yu GM, Huang SL. 2019. First report of anthracnose of *Mangifera indica* caused by *Colletotrichum scovillei* in China. Plant Dis 103:1043. https://doi.org/10.1094/PDIS-11-18-1980-PDN.
18. Yamagishi D, Otani H, Kodama M. 2006. G protein signaling mediates developmental processes and pathogenesis of *Alternaria alternata*. Mol Plant Microbe Interact 19:1280–1288. https://doi.org/10.1094/MPMI-19-1280.
19. Brown NA, Urban M, Van de Meene AM, Hammond-Kosack KE. 2010. The infection biology of *Fusarium graminearum*: defining the pathways of spikelet to spikelet colonization in wheat ears. Fungal Biol 114:555–571. https://doi.org/10.1016/j.funbio.2010.04.006.
20. Kubo Y, Takano Y. 2013. Dynamics of infection-related morphogenesis and pathogenesis in *Colletotrichum orbiculare*. J Gen Plant Pathol 79:233–242. https://doi.org/10.1007/s10327-013-0451-9.
21. Guyon K, Balagué C, Roby D, Raffaele S. 2014. Secretome analysis reveals effector candidates associated with broad-host-range necrotrophy in the fungal plant pathogen *Sclerotinia sclerotiorum*. BMC Genomics 15:336–319. https://doi.org/10.1186/1471-2164-15-336.
22. Chen J-Y, Xiao H-L, Gui Y-J, Zhang D-D, Li L, Bao Y-M, Dai X-F. 2016. Characterization of the *Verticillium dahliae* exoproteome involves in pathogenicity from cotton-containing medium. Front Microbiol 7:1709. https://doi.org/10.3389/fmicb.2016.01709.
23. Fang Y-L, Xia L-M, Wang P, Zhu L-H, Ye J-R, Huang L. 2018. The MAPKKK CgMck1 is required for cell wall integrity, appressorium development, and pathogenicity in *Colletotrichum gloeosporioides*. Genes 9:543. https://doi.org/10.3390/genes9110543.
24. Fernandez J, Orth K. 2018. Rise of a cereal killer: the biology of *Magnaporthe oryzae* biotrophic growth. Trends Microbiol 26:582–597. https://doi.org/10.1016/j.tim.2017.12.007.
25. Gao Y, He L, Li X, Lin J, Mu W, Liu F. 2018. Toxicity and biochemical action of the antibiotic fungicide tetramycin on *Colletotrichum scovillei*. Pestic Biochem Physiol 147:51–58. https://doi.org/10.1016/j.pestbp.2018.02.012.
26. O'Connell RJ, Thon MR, Hacquard S, Amyotte SG, Kleemann J, Torres MF, Damm U, Buiate EA, Epstein L, Alkan N, Altmüller J, Alvarado-Balderrama L, Bauser CA, Becker C, Birren BW, Chen Z, Choi J, Crouch JA, Duvick JP, Farman MA, Gan P, Heiman D, Henrissat B, Howard RJ, Kabbage M, Koch C, Kracher B, Kubo Y, Law AD, Lebrun M-H, Lee Y-H, Miyara I, Moore N, Neumann U, Nordström K, Panaccione DG, Panstruga R, Place M, Proctor RH, Prusky D, Rech G, Reinhardt R, Rollins JA, Rounsley S, Schardl CL, Schwartz DC, Shenoy N, Shirasu K, Sikhakolli UR, Stüber K, et al. 2012. Lifestyle transitions in plant pathogenic *Colletotrichum* fungi deciphered by genome and transcriptome analyses. Nat Genet 44:1060–1065. https://doi.org/10.1038/ng.2372.
27. Latunde-Dada A, O'Connell R, Nash C, Pring R, Lucas J, Bailey J. 1996. Infection process and identity of the hemibiotrophic anthracnose fungus (*Colletotrichum destructivum*) from cowpea (*Vigna unguiculata*. ). Mycol Res 100:1133–1141. https://doi.org/10.1016/S0953-7562(96)80226-7.
28. Gan P, Ikeda K, Irieda H, Narusaka M, O'Connell RJ, Narusaka Y, Takano Y, Kubo Y, Shirasu K. 2013. Comparative genomic and transcriptomic analyses reveal the hemibiotrophic stage shift of *Colletotrichum* fungi. New Phytol 197:1236–1249. https://doi.org/10.1111/nph.12085.
29. Liao CY, Chen MY, Chen YK, Kuo KC, Chung KR, Lee MH. 2012. Formation of highly branched hyphae by *Colletotrichum acutatum* within the fruit cuticles of *Capsicum* spp. Plant Pathol 61:262–270. https://doi.org/10.1111/j.1365-3059.2011.02523.x.
30. De Silva DD, Crous PW, Ades PK, Hyde KD, Taylor PW. 2017. Life styles of *Colletotrichum* species and implications for plant biosecurity. Fungal Biol Rev 31:155–168. https://doi.org/10.1016/j.fbr.2017.05.001.
31. Kim J-O, Choi K-Y, Han J-H, Choi I-Y, Lee Y-H, Kim KS. 2016. The complete mitochondrial genome sequence of the ascomycete plant pathogen *Colletotrichum acutatum*. Mitochondrial DNA A DNA Mapp Seq Anal 27:4547–4548. https://doi.org/10.3109/19401736.2015.1101556.
32. Shin J-H, Han J-H, Park H-H, Fu T, Kim KS. 2019. Optimization of polyethylene glycol-mediated transformation of the pepper anthracnose pathogen *Colletotrichum scovillei* to develop an applied genomics approach. Plant Pathol J 35:575–584. https://doi.org/10.5423/PPJ.OA.06.2019.0171.
33. Kim S, Park S-Y, Kim KS, Rho H-S, Chi M-H, Choi J, Park J, Kong S, Park J, Goh J, Lee Y-H. 2009. Homeobox transcription factors are required for conidiation and appressorium development in the rice blast fungus *Magnaporthe oryzae*. PLoS Genet 5:e1000757. https://doi.org/10.1371/journal.pgen.1000757.
34. Kim KS, Lee Y-H. 2012. Gene expression profiling during conidiation in the rice blast pathogen *Magnaporthe oryzae*. PLoS One 7:e43202. https://doi.org/10.1371/journal.pone.0043202.
35. Shelest E. 2008. Transcription factors in fungi. FEMS Microbiol Lett 286:145–151. https://doi.org/10.1111/j.1574-6968.2008.01293.x.
36. Lavoie H, Hogues H, Whiteway M. 2009. Rearrangements of the transcriptional regulatory networks of metabolic pathways in fungi. Curr Opin Microbiol 12:655–663. https://doi.org/10.1016/j.mib.2009.09.015.
37. Wohlbach DJ, Thompson DA, Gasch AP, Regev A. 2009. From elements to modules: regulatory evolution in Ascomycota fungi. Curr Opin Genet Dev 19:571–578. https://doi.org/10.1016/j.gde.2009.09.007.
38. Montanini B, Levati E, Bolchi A, Kohler A, Morin E, Tisserant E, Martin F, Ottonello S. 2011. Genome-wide search and functional identification of transcription factors in the mycorrhizal fungus *Tuber melanosporum*. New Phytol 189:736–750. https://doi.org/10.1111/j.1469-8137.2010.03525.x.
39. Thiriet-Rupert S, Carrier G, Chénais B, Trottier C, Bougaran G, Cadoret J-P, Schoefs B, Saint-Jean B. 2016. Transcription factors in microalgae: genome-wide prediction and comparative analysis. BMC Genomics 17:282–216. https://doi.org/10.1186/s12864-016-2610-9.
40. Shelest E. 2017. Transcription factors in fungi: TFome dynamics, three major families, and dual-specificity TFs. Front Genet 8:53. https://doi.org/10.3389/fgene.2017.00053.
41. Charoensawan V, Wilson D, Teichmann SA. 2010. Lineage-specific expansion of DNA-binding transcription factor families. Trends Genet 26:388–393. https://doi.org/10.1016/j.tig.2010.06.004.
42. Nowick K, Stubbs L. 2010. Lineage-specific transcription factors and the evolution of gene regulatory networks. Brief Funct Genomics 9:65–78. https://doi.org/10.1093/bfgp/elp056.
43. Lehti-Shiu MD, Panchy N, Wang P, Uygun S, Shiu S-H. 2017. Diversity, expansion, and evolutionary novelty of plant DNA-binding transcription factor families. Biochim Biophys Acta Gene Regul Mech 1860:3–20. https://doi.org/10.1016/j.bbagrm.2016.08.005.
44. Kim J, Cunningham R, James B, Wyder S, Gibson JD, Niehuis O, Zdobnov EM, Robertson HM, Robinson GE, Werren JH, Sinha S. 2010. Functional characterization of transcription factor motifs using cross-species comparison across large evolutionary distances. PLoS Comput Biol 6:e1000652. https://doi.org/10.1371/journal.pcbi.1000652.
45. Levine M, Hoey T. 1988. Homeobox proteins as sequence-specific transcription factors. Cell 55:537–540. https://doi.org/10.1016/0092-8674(88)90209-7.
46. McGinnis W, Krumlauf R. 1992. *Homeobox* genes and axial patterning. Cell 68:283–302. https://doi.org/10.1016/0092-8674(92)90471-n.
47. Lewis EB. 1978. A gene complex controlling segmentation in *Drosophila*. Nature 276:565–570. https://doi.org/10.1038/276565a0.
48. Gehring WJ. 1993. Exploring the homeobox. Gene 135:215–221. https://doi.org/10.1016/0378-1119(93)90068-e.
49. Hull CM, Boily M-J, Heitman J. 2005. Sex-specific homeodomain proteins Sxi1$\alpha$ and Sxi2a coordinately regulate sexual development in *Cryptococcus neoformans*. Eukaryot Cell 4:526–535. https://doi.org/10.1128/EC.4.3.526-535.2005.
50. Zheng W, Zhao X, Xie Q, Huang Q, Zhang C, Zhai H, Xu L, Lu G, Shim W-B, Wang Z. 2012. A conserved homeobox transcription factor Htf1 is required for phialide development and conidiogenesis in *Fusarium* species. PLoS One 7:e45432. https://doi.org/10.1371/journal.pone.0045432.
51. Yokoyama A, Izumitsu K, Sumita T, Tanaka C, Irie T, Suzuki K. 2018. Homeobox transcription factor CoHox3 is essential for appressorium formation in the plant pathogenic fungus *Colletotrichum orbiculare*. Mycoscience 59:353–362. https://doi.org/10.1016/j.myc.2018.02.001.
52. Yokoyama A, Izumitsu K, Irie T, Suzuki K. 2019. The homeobox transcription factor CoHox1 is required for the morphogenesis of infection hyphae

in host plants and pathogenicity in *Colletotrichum orbiculare*. Mycoscience 60:110–115. https://doi.org/10.1016/j.myc.2018.11.001.
53. Liu W, Xie S, Zhao X, Chen X, Zheng W, Lu G, Xu J-R, Wang Z. 2010. A homeobox gene is essential for conidiogenesis of the rice blast fungus *Magnaporthe oryzae*. Mol Plant Microbe Interact 23:366–375. https://doi.org/10.1094/MPMI-23-4-0366.
54. Baroncelli R, Amby DB, Zapparata A, Sarrocco S, Vannacci G, Le Floch G, Harrison RJ, Holub E, Sukno SA, Sreenivasaprasad S, Thon MR. 2016. Gene family expansions and contractions are associated with host range in plant pathogens of the genus *Colletotrichum*. BMC Genomics 17:555. https://doi.org/10.1186/s12864-016-2917-6.
55. Gan P, Narusaka M, Kumakura N, Tsushima A, Takano Y, Narusaka Y, Shirasu K. 2016. Genus-wide comparative genome analyses of *Colletotrichum* species reveal specific gene family losses and gains during adaptation to specific infection lifestyles. Genome Biol Evol 8:1467–1481. https://doi.org/10.1093/gbe/evw089.
56. Baroncelli R, Talhinhas P, Pensec F, Sukno SA, Le Floch G, Thon MR. 2017. The *Colletotrichum acutatum* species complex as a model system to study evolution and host specialization in plant pathogens. Front Microbiol 8: 2001. https://doi.org/10.3389/fmicb.2017.02001.
57. Liang X, Wang B, Dong Q, Li L, Rollins JA, Zhang R, Sun G. 2018. Pathogenic adaptations of *Colletotrichum* fungi revealed by genome wide gene family evolutionary analyses. PLoS One 13:e0196303. https://doi.org/10.1371/journal.pone.0196303.
58. Vonk PJ, Ohm RA. 2018. The role of homeodomain transcription factors in fungal development. Fungal Biol Rev 32:219–230. https://doi.org/10.1016/j.fbr.2018.04.002.
59. Yokotani N, Tsuchida-Mayama T, Ichikawa H, Mitsuda N, Ohme-Takagi M, Kaku H, Minami E, Nishizawa Y. 2014. OsNAC111, a blast disease–responsive transcription factor in rice, positively regulates the expression of defense-related genes. Mol Plant Microbe Interact 27:1027–1034. https://doi.org/10.1094/MPMI-03-14-0065-R.
60. Fernandez J, Wilson RA. 2014. Characterizing roles for the glutathione reductase, thioredoxin reductase and thioredoxin peroxidase-encoding genes of *Magnaporthe oryzae* during rice blast disease. PLoS One 9: e87300. https://doi.org/10.1371/journal.pone.0087300.
61. Yarden O, Veluchamy S, Dickman MB, Kabbage M. 2014. *Sclerotinia sclerotiorum* catalase SCAT1 affects oxidative stress tolerance, regulates ergosterol levels and controls pathogenic development. Physiol Mol Plant Pathol 85:34–41. https://doi.org/10.1016/j.pmpp.2013.12.001.
62. Kim K-T, Jeon J, Choi J, Cheong K, Song H, Choi G, Kang S, Lee Y-H. 2016. Kingdom-wide analysis of fungal small secreted proteins (SSPs) reveals their potential role in host association. Front Plant Sci 7:186. https://doi.org/10.3389/fpls.2016.00186.
63. Choi J, Kim K-T, Jeon J, Lee Y-H. 2013. Fungal plant cell wall-degrading enzyme database: a platform for comparative and evolutionary genomics in fungi and oomycetes. BMC Genomics 14(suppl 5):S7–S10. https://doi.org/10.1186/1471-2164-14-S5-S7.
64. Lelli KM, Slattery M, Mann RS. 2012. Disentangling the many layers of eukaryotic transcriptional regulation. Annu Rev Genet 46:43–68. https://doi.org/10.1146/annurev-genet-110711-155437.
65. Amselem J, Cuomo CA, van Kan JAL, Viaud M, Benito EP, Couloux A, Coutinho PM, de Vries RP, Dyer PS, Fillinger S, Fournier E, Gout L, Hahn M, Kohn L, Lapalu N, Plummer KM, Pradier J-M, Quévillon E, Sharon A, Simon A, ten Have A, Tudzynski B, Tudzynski P, Wincker P, Andrew M, Anthouard V, Beever RE, Beffa R, Benoit I, Bouzid O, Brault B, Chen Z, Choquer M, Collémare J, Cotton P, Danchin EG, Da Silva C, Gautier A, Giraud C, Giraud T, Gonzalez C, Grossetete S, Güldener U, Henrissat B, Howlett BJ, Kodira C, Kretschmer M, Lappartient A, Leroch M, Levis C, et al. 2011. Genomic analysis of the necrotrophic fungal pathogens *Sclerotinia sclerotiorum* and *Botrytis cinerea*. PLoS Genet 7:e1002230. https://doi.org/10.1371/journal.pgen.1002230.
66. Lappin TR, Grier DG, Thompson A, Halliday HL. 2006. *HOX* genes: seductive science, mysterious mechanisms. Ulster Med J 75:23–31.
67. Lelwala RV, Korhonen PK, Young ND, Scott JB, Ades PK, Gasser RB, Taylor PWJ. 2019. Comparative genome analysis indicates high evolutionary potential of pathogenicity genes in *Colletotrichum tanaceti*. PLoS One 14: e0212248. https://doi.org/10.1371/journal.pone.0212248.
68. Ma L-J, van der Does HC, Borkovich KA, Coleman JJ, Daboussi M-J, Di Pietro A, Dufresne M, Freitag M, Grabherr M, Henrissat B, Houterman PM, Kang S, Shim W-B, Woloshuk C, Xie X, Xu J-R, Antoniw J, Baker SE, Bluhm BH, Breakspear A, Brown DW, Butchko RAE, Chapman S, Coulson R, Coutinho PM, Danchin EGJ, Diener A, Gale LR, Gardiner DM, Goff S, Hammond-Kosack KE, Hilburn K, Hua-Van A, Jonkers W, Kazan K, Kodira CD, Koehrsen M, Kumar L, Lee Y-H, Li L, Manners JM, Miranda-Saavedra D, Mukherjee M, Park G, Park J, Park S-Y, Proctor RH, Regev A, Ruiz-Roldan MC, Sain D, et al. 2010. Comparative genomics reveals mobile pathogenicity chromosomes in *Fusarium*. Nature 464:367–373. https://doi.org/10.1038/nature08850.
69. Gunnell PS, Gubler WD. 1992. Taxonomy and morphology of *Colletotrichum* species pathogenic to strawberry. Mycologia 84:157–165. https://doi.org/10.2307/3760246.
70. Leandro LF, Gleason ML, Nutter FW, Jr, Wegulo SN, Dixon PM. 2001. Germination and sporulation of *Colletotrichum acutatum* on symptomless strawberry leaves. Phytopathology 91:659–664. https://doi.org/10.1094/PHYTO.2001.91.7.659.
71. Takahara H, Hacquard S, Kombrink A, Hughes HB, Halder V, Robin GP, Hiruma K, Neumann U, Shinya T, Kombrink E, Shibuya N, Thomma BPHJ, O'Connell RJ. 2016. *Colletotrichum higginsianum* extracellular LysM proteins play dual roles in appressorial function and suppression of chitin-triggered plant immunity. New Phytol 211:1323–1337. https://doi.org/10.1111/nph.13994.
72. Gong B-Q, Wang F-Z, Li J-F. 2020. Hide-and-seek: chitin-triggered plant immunity and fungal counterstrategies. Trends Plant Sci 25:805–816. https://doi.org/10.1016/j.tplants.2020.03.006.
73. Li J, Fokkens L, Conneely LJ, Rep M. 2020. Partial pathogenicity chromosomes in *Fusarium oxysporum* are sufficient to cause disease and can be horizontally transferred. Environ Microbiol 22:4985–5004. https://doi.org/10.1111/1462-2920.15095.
74. Wang D, Tian L, Zhang D-D, Song J, Song S-S, Yin C-M, Zhou L, Liu Y, Wang B-L, Kong Z-Q, Klosterman SJ, Li J-J, Wang J, Li T-G, Adamu S, Subbarao KV, Chen J-Y, Dai X-F. 2020. Functional analyses of small secreted cysteine-rich proteins identified candidate effectors in *Verticillium dahliae*. Mol Plant Pathol 21:667–685. https://doi.org/10.1111/mpp.12921.
75. Howard RJ, Valent B. 1996. Breaking and entering: host penetration by the fungal rice blast pathogen *Magnaporthe grisea*. Annu Rev Microbiol 50:491–513. https://doi.org/10.1146/annurev.micro.50.1.491.
76. Veneault-Fourrey C, Barooah M, Egan M, Wakley G, Talbot NJ. 2006. Autophagic fungal cell death is necessary for infection by the rice blast fungus. Science 312:580–583. https://doi.org/10.1126/science.1124550.
77. Bao W, Kojima KK, Kohany O. 2015. RepBase update, a database of repetitive elements in eukaryotic genomes. Mob DNA 6:11. https://doi.org/10.1186/s13100-015-0041-9.
78. Katoh K, Standley DM. 2013. MAFFT multiple sequence alignment software version 7: improvements in performance and usability. Mol Biol Evol 30:772–780. https://doi.org/10.1093/molbev/mst010.
79. Capella-Gutiérrez S, Silla-Martínez JM, Gabaldón T. 2009. trimAl: a tool for automated alignment trimming in large-scale phylogenetic analyses. Bioinformatics 25:1972–1973. https://doi.org/10.1093/bioinformatics/btp348.
80. Fornes O, Castro-Mondragon JA, Khan A, van der Lee R, Zhang X, Richmond PA, Modi BP, Correard S, Gheorghe M, Baranašić D, Santana-Garcia W, Tan G, Chèneby J, Ballester B, Parcy F, Sandelin A, Lenhard B, Wasserman WW, Mathelier A. 2020. JASPAR 2020: update of the open-access database of transcription factor binding profiles. Nucleic Acids Res 48:D87–D92. https://doi.org/10.1093/nar/gkz1001.
81. Ambrosini G, Groux R, Bucher P. 2018. PWMScan: a fast tool for scanning entire genomes with a position-specific weight matrix. Bioinformatics 34: 2483–2484. https://doi.org/10.1093/bioinformatics/bty127.
82. Ye J, Zhang Y, Cui H, Liu J, Wu Y, Cheng Y, Xu H, Huang X, Li S, Zhou A, Zhang X, Bolund L, Chen Q, Wang J, Yang H, Fang L, Shi C. 2018. WEGO 2.0: a web tool for analyzing and plotting GO annotations, 2018 update. Nucleic Acids Res 46:W71–W75. https://doi.org/10.1093/nar/gky400.
83. Park J, Kong S, Kim S, Kang S, Lee Y. 2014. Roles of forkhead-box transcription factors in controlling development, pathogenicity, and stress response in *Magnaporthe oryzae*. Plant Pathol J 30:136–150. https://doi.org/10.5423/PPJ.OA.02.2014.0018.
84. Han J-H, Lee H-M, Shin J-H, Lee Y-H, Kim KS. 2015. Role of the *MoYAK 1* protein kinase gene in *Magnaporthe oryzae* development and pathogenicity. Environ Microbiol 17:4672–4689. https://doi.org/10.1111/1462-2920.13010.
85. Han J-H, Shin J-H, Lee Y-H, Kim KS. 2018. Distinct roles of the *YPEL* gene family in development and pathogenicity in the ascomycete fungus *Magnaporthe oryzae*. Sci Rep 8:14461. https://doi.org/10.1038/s41598-018-32633-6.
86. Yu J-H, Hamari Z, Han K-H, Seo J-A, Reyes-Domínguez Y, Scazzocchio C. 2004. Double-joint PCR: a PCR-based molecular tool for gene manipulations in filamentous fungi. Fungal Genet Biol 41:973–981. https://doi.org/10.1016/j.fgb.2004.08.001.

87. Goh J, Jeon J, Kim KS, Park J, Park S-Y, Lee Y-H. 2011. The PEX7-mediated peroxisomal import system is required for fungal development and pathogenicity in *Magnaporthe oryzae*. PLoS One 6:e28220. https://doi.org/10.1371/journal.pone.0028220.
88. Fu T, Kim J-O, Han J-H, Gumilang A, Lee Y-H, Kim KS. 2018. A small GTPase RHO2 plays an important role in preinfection development in the rice blast pathogen *Magnaporthe oryzae*. Plant Pathol J 34:470–479. https://doi.org/10.5423/PPJ.OA.04.2018.0069.
89. Park S-Y, Choi J, Lim S-E, Lee G-W, Park J, Kim Y, Kong S, Kim SR, Rho H-S, Jeon J, Chi M-H, Kim S, Khang CH, Kang S, Lee Y-H. 2013. Global expression profiling of transcription factor genes provides new insights into pathogenicity and stress responses in the rice blast fungus. PLoS Pathog 9:e1003350. https://doi.org/10.1371/journal.ppat.1003350.
90. Chi M-H, Park S-Y, Lee Y-H. 2009. A quick and safe method for fungal DNA extraction. Plant Pathol J 25:108–111. https://doi.org/10.5423/PPJ.2009.25.1.108.
91. Livak KJ, Schmittgen TD. 2001. Analysis of relative gene expression data using real-time quantitative PCR and the $2^{-\Delta\Delta}CT$ method. Methods 25:402–408. https://doi.org/10.1006/meth.2001.1262.
92. Fu T, Park G-C, Han JH, Shin J-H, Park H-H, Kim KS. 2019. *MoRBP9* encoding a Ran-binding protein microtubule-organizing center is required for asexual reproduction and infection in the rice blast pathogen *Magnaporthe oryzae*. Plant Pathol J 35:564–574. https://doi.org/10.5423/PPJ.OA.07.2019.0204.
93. Kim KS, Min J-Y, Dickman MB. 2008. Oxalic acid is an elicitor of plant programmed cell death during *Sclerotinia sclerotiorum* disease development. Mol Plant Microbe Interact 21:605–612. https://doi.org/10.1094/MPMI-21-5-0605.
94. Dangol S, Chen Y, Hwang BK, Jwa N-S. 2019. Iron-and reactive oxygen species-dependent ferroptotic cell death in rice-*Magnaporthe oryzae* interactions. Plant Cell 313. 189–209. https://doi.org/10.1105/tpc.18.00535.
95. Rios JJ, Carrasco-Gil S, Abadía A, Abadía J. 2016. Using Perls staining to trace the iron uptake pathway in leaves of a Prunus rootstock treated with iron foliar fertilizers. Front Plant Sci 7:893. https://doi.org/10.3389/fpls.2016.00893.
96. Chen S, Zhou Y, Chen Y, Gu J. 2018. fastp: an ultra-fast all-in-one FASTQ preprocessor. Bioinformatics 34:i884–i890. https://doi.org/10.1093/bioinformatics/bty560.
97. Kim D, Paggi JM, Park C, Bennett C, Salzberg S. 2019. Graph-based genome alignment and genotyping with HISAT2 and HISAT-genotype. Nat Biotechnol 37:907–915. https://doi.org/10.1038/s41587-019-0201-4.
98. Kovaka S, Zimin AV, Pertea GM, Razaghi R, Salzberg SL, Pertea M. 2019. Transcriptome assembly from long-read RNA-seq alignments with StringTie2. Genome Biol 20:278–213. https://doi.org/10.1186/s13059-019-1910-1.
99. Love MI, Huber W, Anders S. 2014. Moderated estimation of fold change and dispersion for RNA-seq data with DESeq2. Genome Biol 15:550–521. https://doi.org/10.1186/s13059-014-0550-8.